ILLINOIS CENTER FOR TRANSPORTATION

Report No. FHWA-ICT-26-002

Spatial and Temporal Load Distribution in Steel Bridge Superstructures (Vol. I): Agency Survey and Preliminary Numerical Modeling of Skewed Steel I-Girder Bridges for Field Instrumentation

Siang Zhou
Ricardo Dorado
James M. LaFave
Larry A. Fahnestock

ICT Project R27-194

February 2026

ISSN: 0197-9191
ICT Series Report No. 26-002
https://doi.org/10.36501/0197-9191/26-002

TECHNICAL REPORT DOCUMENTATION PAGE

1. Report No.	2. Government Accession No.	3. Recipient's Catalog No.
FHWA-ICT-26-002	N/A	N/A

4. Title and Subtitle	5. Report Date
Spatial and Temporal Load Distribution in Steel Bridge Superstructures (Vol. I): Agency Survey and Preliminary Numerical Modeling of Skewed Steel I-Girder Bridges for Field Instrumentation	February 2026
	6. Performing Organization Code N/A

7. Authors	8. Performing Organization Report No.
Siang Zhou (https://orcid.org/0000-0002-1540-5698), Ricardo Dorado (https://orcid.org/0000-0002-5906-4792), James M. LaFave (https://orcid.org/0000-0001-6514-2163), Larry A. Fahnestock (https://orcid.org/0000-0003-3172-2260)	ICT-26-002 UILU-2026-2002

9. Performing Organization Name and Address	10. Work Unit No.
Illinois Center for Transportation Department of Civil and Environmental Engineering University of Illinois Urbana-Champaign 205 North Mathews Avenue, MC-250 Urbana, IL 61801	N/A
	11. Contract or Grant No. R27-194

12. Sponsoring Agency Name and Address	13. Type of Report and Period Covered
Illinois Department of Transportation (SPR) Bureau of Research 126 East Ash Street Springfield, IL 62704	Interim Report 7/1/18–2/28/26
	14. Sponsoring Agency Code

15. Supplementary Notes

Conducted in cooperation with the U.S. Department of Transportation, Federal Highway Administration.
https://doi.org/10.36501/0197-9191/26-002

16. Abstract

Highly skewed steel I-girder bridges are used commonly across the US, especially in congested areas, despite complications in their analysis, design, and construction. Systematic investigation of skewed steel I-girder superstructure response, load distribution, and deformation through field monitoring and numerical simulation is needed, including analysis of bridges under construction, short-term live load, and long-term thermal and traffic loads. AASHTO's load and resistance factor design specification allows for line girder analysis with defined live load distribution factors (considering effects of skew between 30° and 60°) when designing non-curved steel bridges. When considering lateral behavior of skewed bridges, AASHTO provides suggestions for design values of flange lateral bending stress in addition to line girder analysis when bridge skew exceeds 20° for certain cross-frame layouts. This skew limit is 45° in Illinois Department of Transportation's "Bridge Design Manual." When designing bridges for lateral bending during deck placement, AASHTO suggests equations to conservatively estimate flange lateral bending moments caused by eccentric loading from an overhang acting on an exterior girder top flange, in the absence of a refined analysis. Efficiency of the simplified design approaches and skew consideration in current standard design practice needs to be further evaluated through field monitoring and companion numerical studies. The research project partially described in this report was initiated in Illinois to investigate demands, load distribution, and static and dynamic responses of composite steel skewed I-girder bridge superstructures during construction and after bridges are in service. Two skewed steel I-girder bridges (41° and 45°), with stub and integral abutments, respectively, were studied through field monitoring and numerical simulations. This report documents the initial phases of the research: a survey to understand practices used and challenges faced by state transportation agencies when designing and constructing skewed steel I-girder bridges, information about and field instrumentation of the two monitored bridges, methods for 3D finite element analysis, and preliminary analysis conducted to guide field instrumentation planning of the bridges.

17. Key Words	18. Distribution Statement
Skewed Bridge, Steel I-Girder Bridge, Flange Lateral Bending, Field Monitoring, Numerical Simulation, Deck Placement, Live Load, Thermal Effect	No restrictions. This document is available through the National Technical Information Service, Springfield, VA 22161.

19. Security Classif. (of this report)	20. Security Classif. (of this page)	21. No. of Pages	22. Price
Unclassified	Unclassified	48	N/A

ACKNOWLEDGMENT, DISCLAIMER, MANUFACTURERS' NAMES

This publication is based on the results of **ICT-R27-194: Evaluation of Spatial and Temporal Load Distribution in Steel Bridge Superstructures**. ICT-R27-194 was conducted in cooperation with the Illinois Center for Transportation; the Illinois Department of Transportation; and the U.S. Department of Transportation, Federal Highway Administration.

Members of the Technical Review Panel (TRP) were the following:

- Mark Shaffer, TRP Chair, Illinois Department of Transportation
- Andrew Bauer, Illinois Department of Transportation
- Ruben Boehler, Illinois Department of Transportation
- Nick Lombardi, Federal Highway Administration
- Peter Pascua, Illinois Department of Transportation
- Kevin Riechers, Illinois Department of Transportation

EXECUTIVE SUMMARY

Highly skewed steel I-girder bridges are used commonly across the US, especially in congested areas, despite complexities in their analysis, design, and construction. Bridge superstructure behavior is complicated by the effects of skew due to additional load paths introduced via the skewed supports and through load transfer at cross-frames and the deck. Field-monitoring efforts focusing on large-scale skewed steel I-girder bridge superstructures are sparse. In previous research studying in-service skewed steel I-girder bridges, superstructure response under short-term live load and long-term thermal variation were sometimes not well predicted by current analysis procedures and design requirements. Skewed steel I-girder bridges also exhibit unique behavior under construction, especially during deck placement when the superstructure is in pre-composite condition. Prior studies have focused on constructability regarding movements of superstructure components, and evaluation of bridge strength limit states—including the lateral behavior of steel I-girder and cross-frame systems under deck placement—have largely relied on numerical simulations. Skewed steel I-girder superstructure response, load distribution, and deformation under construction; short-term live load; and long-term large thermal load and cyclic traffic load need to be more thoroughly studied. Field monitoring is valuable to enhance understanding of skewed steel I-girder bridge behavior and assist development of reliable numerical simulation methods.

The American Association of State Highway and Transportation Officials (AASHTO) *Load and Resistance Factor* (*LRFD) Bridge Design Specifications* allows for line girder analysis with defined live load distribution factors when designing non-curved steel bridges. The effect of skew (considered from 30° to 60°) is included in design through extra coefficients calculated from equations related to skew angle when determining live load distribution factors (LLDF) for bridges with steel girders using approximate methods of analysis. Efficiency of the simplified design approaches and skew consideration in LLDF needs to be further evaluated through field monitoring and companion numerical simulations. For skewed bridge lateral behavior, AASHTO provides suggestions for design values of flange lateral bending stress in addition to line girder analysis when bridge skew exceeds 20° for certain cross-frame layouts. The *Bridge Design Manual* by Illinois Department of Transportation (IDOT) requires additional lateral bending stress for bridges skewed more than 45°. For bridges with skew exceeding 60°, a higher level of analysis is often required, with cross-frames considered primary members in design. Neither the magnitude of additional lateral stress nor the associated skew limits are particularly well understood, so more study is needed to refine and support this analysis and design approach. When designing bridges for lateral bending during deck placement, in the absence of a refined analysis, AASHTO suggests equations to conservatively estimate flange lateral bending moments caused by eccentric loading from an overhang acting on an exterior girder. The efficiency of such approximation also needs to be further evaluated.

The current project was initiated in Illinois to address the needs of investigating demands, load distribution, and dynamic response of composite skewed I-girder bridge superstructures during construction and after bridges are in service. Highly skewed steel I-girder bridges with stub and integral abutments were monitored in the field and analyzed with combined field measurements and numerical simulations under concrete dead load, traffic live load, and thermal load. The project

employed long-term field monitoring of skewed steel I-girder bridges and 3D finite element analysis of the monitored bridges.

This report documents the initial phases of the research. A survey was formulated and distributed across the US to understand practices used and challenges faced by state transportation agencies when designing and constructing skewed steel I-girder bridges. Findings from the responses of 23 state agencies illuminate issues, concerns, and current practices related to design, construction, and service life of those bridges. The agency survey guided the objectives of the research and informed the selection of two bridges in Champaign, Illinois, for field monitoring to provide enhanced understanding of the effects of skew on bridge superstructure behavior. Two steel I-girder bridges skewed 41° and 45°, with stub and integral abutments, respectively, were monitored in the field during construction and after the bridges were in service. Critical girder cross-sections and cross-frames were instrumented with strain gauges using a data acquisition system with a high sampling frequency (up to 20 Hz). In addition, key girder end rotations and all bridge corner movements were monitored. Temperature variation was recorded from all sensors. Three-dimensional finite element analysis methods have been improved through iterations of model validation after field monitoring started, and some of the refined modeling methods are presented as part of this report. Before the start of data collection, numerical simulation techniques were initially validated with prior research, and preliminary analysis was conducted to guide field instrumentation planning.

TABLE OF CONTENTS

LIST OF FIGURES

LIST OF TABLES

CHAPTER 1: INTRODUCTION

Highly skewed steel I-girder bridges are used commonly across the US, especially in congested areas, despite complications in their analysis and design during construction and after bridges are in service. Figure 1 presents a plan view of a typical skewed steel I-girder bridge in a database provided by the Illinois Department of Transportation (IDOT), recording bridges (total of 184) designed and constructed by IDOT between 2005 and 2020. The two-span continuous bridge was constructed in three stages, with concrete placed in two phases during each stage. This bridge, Mattis Avenue over I-74 (Mattis-74), is one of the bridges eventually selected for field monitoring in the current research, the details of which will be discussed in this report. This chapter introduces the background of the current research, including previous studies and standard design practices, and presents the research covered and outline of this report.

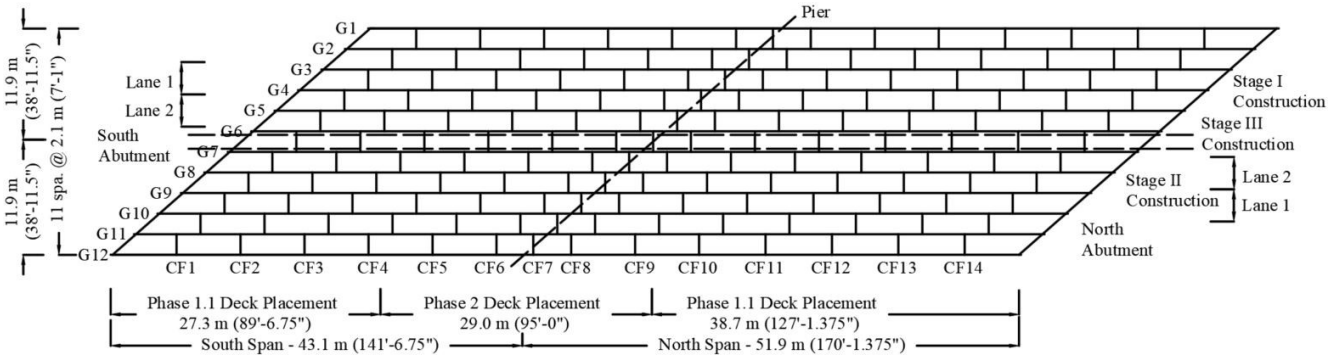

Figure 1. Plan view. Representative IDOT skewed steel I-girder bridge (Mattis-74).

RESEARCH BACKGROUND: LITERATURE REVIEW

In-Service Skewed Steel I-Girder Bridges

In-service live load distribution and long-term thermal-induced behavior of steel I-girder bridges can be complicated for bridges designed with skew, both when expansion joints or integral abutments are used. Field-monitoring efforts on large-scale in-service skewed steel I-girder bridges have focused on capturing the behavior of integral abutment bridges, studying the response of cross-frames and adjacent girders under live load, and recording the behavior of curved-girder bridges. Skewed steel I-girder bridges have been observed with structural response not predicted by current design guidelines, including unexpectedly large stress variations in bottom flanges of I-girders during long-term data collection (LaFave et al. 2021), web out-of-plane bending (also referred to as web warping) of steel I-girders and biaxial bending of cross-frames during live load testing (McConnell et al. 2016), and large thermally induced girder bottom flange stresses (Greimann et al. 2014). Systematic understanding of short-term load distribution and long-term thermal response of in-service skewed steel I-girder bridge superstructures could be enhanced with new field data on superstructure behavior of straight skewed steel I-girder bridges.

Investigation on load distribution of bridges with skewed support has also been a growing topic, especially studies regarding skewed deck bridges (Theoret et al. 2012). For composite skewed bridges

with steel I-girders, lateral load distribution under the combined effect of a composite deck-girder and cross-frame system is more complicated, and existing studies have focused on effects of cross-frames on development of girder stress (McConnell et al. 2020). Additional work to separately investigate superstructure load distribution regarding girder major-axis and lateral bending is needed, especially with support from field test results. Lateral bending and web plate out-of-plane behavior should be further investigated for all girders, especially for bridges employing staged construction where a more slender half-bridge—compared to the eventual full-size bridge—is first loaded.

In addition to bridge behavior under static loads, field data are needed to expand understanding of dynamic bridge response under moving live loads (Deng et al. 2015). Dynamic properties and dynamic load allowance (DLA) (or dynamic impact factor [IM]) of skewed bridges have been evaluated in prior research through mostly numerical and analytical simulations (Deng and Phares 2016; Huang 2001; Huang et al. 1995; Sağlık et al. 2018). Furthermore, very limited evaluation of DLA has been performed regarding skewed bridges with I-girders (Almoosi et al. 2021).

Skewed Steel I-Girder Bridges under Construction

Skewed steel I-girder bridges also exhibit unique behavior under construction, especially development of lateral bending during deck placement when the superstructure is in pre-composite condition. Previous research has focused on constructability regarding movements of superstructure components, including observations of large out-of-plane deformation in girder web plates and twist of the girder system, undesirable girder differential deflections, increasing girder end rotations with increasing bridge skew, and development of uneven deck thickness (Aktan and Attanayake 2020; Choo et al. 2005; Freeseman et al. 2014; Morera and Sumner 2020; Yang et al. 2010). Studies evaluating superstructure strength focused on other practical aspects of construction rather than skew, including girder stress variation owing to deck placement direction and reduction of concrete stress by conducting phased deck placement (Choo et al. 2005; Salah 2020). Even though previous research has demonstrated the existence of considerable girder lateral behavior for pre-composite skewed steel systems during deck placement, investigations on lateral bending stress due to skew are still needed.

Two sources of flange lateral bending for a straight I-girder bridge were identified in previous research (Sanchez 2011; White et al. 2012): from overhang loading (considered by AASHTO, as discussed in the next section) in the vicinity of cross-frames and from support skew. The kinematics explaining girder lateral movement caused by support skew were presented, and finite element analysis (FEA) demonstrated large flange lateral bending stresses near bridge supports, except when total dead load fit was used. However, these studies focused on understanding girder end layover of a skewed bridge and comparing flange lateral bending when using different cross-frame detailing methods, instead of quantifying contribution of skew on flange lateral bending stress. The FEA conducted for these studies modeled girder flanges using beam elements without considering localized plate bending effects, and boundary conditions were defined based on simple idealizations of typical support conditions.

RESEARCH BACKGROUND: STANDARD DESIGN PRACTICE

Consideration of skew in bridge design and construction has gone through modifications in recent years, and it is still an active research topic that could bring improvement to the safety and efficiency of bridge design. Research in the past decade for these bridges has motivated the evolution of standard design procedures, including girder and cross-frame demand estimation and detailing recommendations (White and Jamath 2020). AASHTO (2017) allows for line girder analysis with defined live load distribution factors, per Article 4.6.2.2, when designing non-curved steel bridges. The effect of skew (considered from 30° to 60°) is considered through extra coefficients calculated from equations related to skew angle when determining live load distribution factors (LLDF) for bridges with steel girders using approximate methods of analysis. Efficiency of line girder analysis and the application of LLDF on diverse types of bridges have been well evaluated by prior research (Barr et al. 2001; Choi et al. 2019; Dicleli and Yalcin 2018; Khaloo and Mirzabozorg 2003; Mohseni et al. 2018; Nouri and Ahmadi 2012; Razzaq et al. 2021; Terzioglu et al. 2017). However, the studies were largely based on numerical analysis, which especially limited the accuracy in consideration of bridge skew. Therefore, further evaluation of the widely used design methods through field monitoring of considerably skewed bridges will be beneficial.

Lateral bending behavior of skewed steel I-girder bridges is considered by AASHTO (2017, Commentary C6.10.1), through an additional flange lateral bending stress of 69 MPa (10 ksi), for interior girders in the absence of calculated values from a refined analysis when bridge skew exceeds 20°. The AASHTO suggestion for lateral stress of exterior girders is lower—14 MPa or 52 MPa (2 ksi or 7.5 ksi), depending on the layout of cross-frames in a skewed bridge. Bridge response is considered under the same dynamic effect under live load regardless of skew. AASHTO requires DLA of 33% when fatigue is not considered (AASHTO 2017, Table 3.6.2.1-1), which could be subject to variation based on specific analysis considering types of loading, vehicle configuration, and bridge geometry.

Most transportation agencies follow the AASHTO LRFD suggestions. However, special requirements from individual state transportation agencies may reflect distinct needs and recent research findings of the states. The IDOT *Bridge Manual* (2012) does not require the use of additional lateral stress when a bridge is skewed less than 45°. IDOT uses additional lateral bending stress of 69 MPa (10 ksi), or half that value for fatigue load stress, for all girders when the structure is skewed between 45° and 60°. The new IDOT *Bridge Manual* (2023) states that a higher level of analysis is required when bridges are skewed more than 60°, during which cross-frames need to be considered primary members in design. An independent analysis contracted by the department, which studied live load distributions factors, was conducted in support of such policy (URS Corporation 2016), which considered variations in beam spacing, beam depth, substructure skew angle, and bridge span-to-width aspect ratio. However, effects on bridge behavior from abutment type, as well as from types and layouts of cross-frames, were not examined. That study also recommended standard diaphragm details, even though part of the diaphragm force exceeded current AASHTO assumptions without a refined analysis. The URS study did not separately examine lateral behavior of interior and exterior girders, and the LLDF was only studied for bridge exterior girders. Further examination of these aspects through field monitoring and analysis with validated numerical models could enhance safety and efficiency in design recommendations.

When considering bridge lateral bending during deck placement, in the absence of a refined analysis, AASHTO (2017) Commentary C6.10.3.4 suggests equations to conservatively estimate flange lateral bending moments caused by eccentric loading from an overhang acting on an exterior girder top flange. The effect of skew is then separately considered in Commentary C6.10.1, as mentioned above. The relatively coarse estimation of skew-induced flange lateral bending response needs to be more thoroughly evaluated, especially for a pre-composite (steel only) bridge superstructure system during deck placement. Previous research suggested improvements in calculation of flange lateral bending stress and cross-frame force for pre-composite bridges by considering refined cross-frame stiffness in 2D-grid analysis and then applying more accurate cross-frame forces to efficiently estimate girder flange lateral bending (White et al. 2012). The accuracy of such calculation relies on appropriate approximation of cross-frame forces, and bridge skew is included in 2D-grid analysis instead of explicitly studied with respect to lateral bending stress.

CURRENT RESEARCH AND REPORT OUTLINE

The current project was initiated in Illinois to investigate demands, load distribution, and dynamic response of a composite skewed I-girder bridge superstructure during construction and after bridges are in service. Highly skewed stub abutment bridges and integral abutment bridges with steel I-girders were analyzed under concrete dead load, traffic live load, and thermal load. The project employs long-term field monitoring of skewed steel I-girder bridges and 3D FEA of the monitored bridges.

The project is divided into four tasks. This report presents the early stages of the research: summary of agency survey (Chapter 2), configuration of field monitoring (Chapter 3), framework for numerical simulation (Chapter 4), and preliminary numerical simulation that assisted instrumentation (Chapter 5).

- **Task 1: Literature review and agency survey**. A review of the existing research literature and typical design practices for steel I-girder bridges was conducted to inform, guide, and provide context to the current research. A summary of the literature review is discussed in Chapter 1 and throughout the report. In addition, a targeted survey was distributed to US state agencies to assess how load distribution and secondary effects are considered in the design and construction of steel I-girder bridges, with a particular focus on skewed bridges. Chapter 2 presents findings from the agency survey. The survey guided the project planning and informed the selection of bridges for instrumentation.

- **Task 2: Field monitoring**. Informed by findings from the agency survey, two new IDOT steel I-girder bridges were selected for a long-term field-monitoring campaign to collect data that document construction and in-service behavior of the bridges. Two bridges skewed 41° and 45° (one with stub abutments and the other with integral abutments) were monitored in the field. Strain and temperature variation at critical girder cross-sections and cross-frames were monitored, and bridge global movement (girder end rotations and bridge in-plan displacements) was captured. Chapter 3 presents information about the selected bridges, detailed instrumentation plans, and the processing scheme of field measurements.

- **Task 3: Numerical simulation**. Numerical simulations were carried out in the current research to enhance understanding of field measurements by modeling the bridges under field monitoring and to provide insights into geometric effects on skewed steel I-girder bridge behavior through parametric studies. Three-dimensional FEA methods have been developed since the beginning of the project. Before bridges were in place, numerical simulations were validated with prior research, and instrumentation placement was determined according to a set of preliminary numerical simulations. Iterations to improve the accuracy of computational modeling have been conducted with field measurements after data collection started. Chapter 4 presents numerical modeling methods, and Chapter 5 presents the preliminary numerical simulations.

- **Task 4: Design recommendations**. After synthesizing the prior three tasks, observations and insights on the behavior of skewed steel I-girder bridges will be summarized, and analysis, design, and construction guidelines will be proposed to implement the research results in practice. Field monitoring, companion numerical simulations, parametric study results, and observations on bridge behavior will be presented in a subsequent project report.

CHAPTER 2: SUMMARY OF AGENCY SURVEY

A survey was created and distributed to US state transportation agencies to systematically gather information about skewed steel I-girder bridges (i.e., in-service behavior, general design practice, and guidelines for design and construction) to help guide the research. Twenty-three responses were received from various state agencies (Figure 2), which is a similar response rate to that of another recent survey involving bridge approach slabs (Fahnestock et al. 2022). Survey results presented in this section, as supplemented by referenced state agency design guidelines (FDOT 2021; NeDOR 2016; PennDOT 2016, 2019; TxDOT 2018, 2019; UDOT 2017) and previous research (White et al. 2012; White and Jamath 2020) recommended by the respondents, shed light on areas where further understanding could increase safety and efficiency of bridge designs.

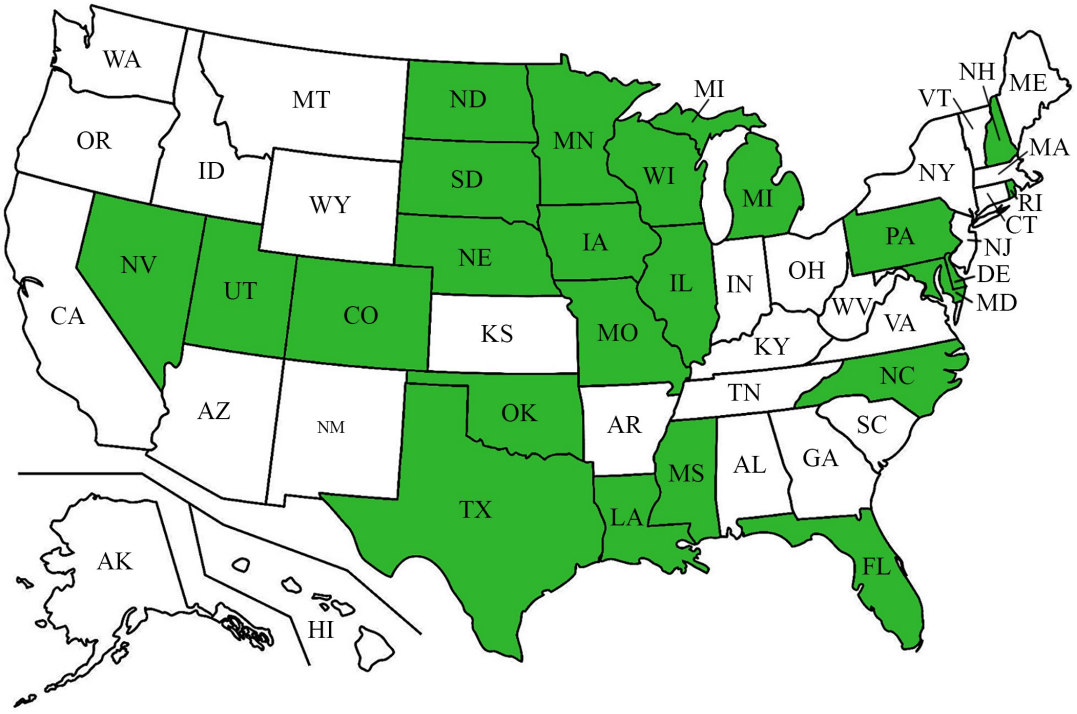

Figure 2. Map. States that responded to agency survey (shaded).

GENERAL INFORMATION AND LIMITS OF SKEWED STEEL I-GIRDER BRIDGES

Steel I-girder bridges comprise a significant portion of newly designed and constructed bridges, especially among highway bridges and long-span or wide bridges. Eight states reported that over 20% of bridges designed or constructed between 2013 and 2018 had steel girders, with three states reporting around or over 50%. For instance, of the slab-on-girder bridges designed and constructed by IDOT between 2013 and 2018, 80% were steel bridges.

Even though almost all responding agencies mentioned they would prefer straight girder bridges (with no skew), the need for skewed bridges is sometimes inevitable. For the five-year period from 2013 to 2018, 70% of respondents reported having built steel bridges with skew larger than 45°, and

more than a quarter of respondents indicated that at least 10% of their recently built steel bridges have skew over 45°. In addition, 65% of responding states reported that at least 25% of their steel bridges had skew over 20°, which is the skew threshold currently recommended by AASHTO for consideration of additional flange lateral bending stress. In the IDOT database, 14% of bridges had skew equal to or larger than 30°, and 4% of bridges had skew greater than 45°. Table 1 presents preferred or required limits of skew reported by state agencies when new bridges are designed, even though some special cases of their reported bridges had skews even larger than the preferred limit.

Table 1. Preferred Skew Angle Limits When Designing New Steel I-Girder Bridges

Skew Angle Limit	Limit Specification	Stage Agencies
15°	Preferred	New Hampshire
30°	Preferred	Pennsylvania, Utah
35°	Required for integral abutment bridges	South Dakota
40°	Preferred	Delaware
45°	Preferred	Rhode Island
45°	Required	Mississippi
50°	Preferred	Colorado, Florida
60°	Preferred	Utah
60°	Required	Louisiana

Limits on span length for skewed steel girder bridges are reported to range from 61 m (200 ft) to 122 m (400 ft)—e.g., 69 m (225 ft) for single-span bridges and 76 m (250 ft) for multi-span continuous bridges (Utah DOT). General practice for bridge width limit ranges from 24 m (80 ft) to 30 m (100 ft), and in some states additional measures are taken—such as longitudinal deck joints (IDOT) or extra design review (South Dakota DOT)—for wider bridges.

In the current research project, steel I-girder bridges skewed around or above 45°, with reasonably long span length, moderate bridge width, and either stub abutments or integral abutments, were the target parameters of interest to help further understand the effect of skew on steel I-girder bridge superstructure behavior.

PERFORMANCE OF SKEWED STEEL I-GIRDER BRIDGES

Behavior of skewed bridges, especially when heavily skewed (over 45°), is more complicated both in load distribution and bridge thermal response (as well as regarding fatigue-related issues and constructability concerns). Typical critical performance issues and concerns about skewed steel I-girder bridges, as observed by the state agencies, are recorded in Table 2, most of which are related to bridge skew while some evolve with time and/or temperature variation. For some observations, the causes are understood, whereas other potential causes were either not mentioned or are not clear based on current knowledge. The scope of the current research was formed to gain better understanding of the issues reported in the agency survey, especially where causes are not clear, through field monitoring and numerical simulation.

Table 2. Critical Performance Concerns Observed in Skewed Steel I-Girder Bridges

Component	State Agency	Performance Concern	Cause	Skew Related	Evolves with Time or Temperature
Steel Components	Colorado, Maryland, Michigan, Wisconsin	Fatigue crack at bottom of cross-frame stiffeners, especially in older bridges	Out-of-plane bending due to details of web gap at intermediate stiffener plates	Skew > 45°	Yes
	North Carolina	Girder web deformation	Not mentioned	Yes	No
	Illinois, North Carolina	Large lateral stress variation at girder bottom flange	Not clear	Yes	Not clear
Concrete Deck	Florida, Minnesota, Missouri	Concrete cracks, especially at obtuse and acute corners	Not mentioned	Especially skew > 45°	Not mentioned
	South Dakota	Slab cracks in skewed IABs	Bridge longitudinal expansion and contraction	Yes	Not mentioned
Bridge Global Movement	Illinois	Large global response under temperature changes and traffic, especially at bridge corners	Not mentioned	Yes	Yes
	Maryland	Bridge shifts transversely, breaking anchor bolts	Skewed bridge non-uniform expansion under uneven heating	Yes	Yes
	Delaware, Maryland, Nebraska, Utah	Roadway joint seals (especially sawtooth joints) can experience different joint gap dimensions from one end to the other and might fall out	Not mentioned	Yes	Yes
Construction Phase	Illinois, Louisiana	Bridge “walking” during deck pour	Differential deflections between beams	Skew > 45°	No
	Illinois, Mississippi	Extra locked-in stress for girders	Improper fit-up	Yes	No
	Illinois, Texas	Deck might be poured too thin	Beam final top flange elevation might deflect improperly	Yes	No
	Florida	Bearing uplift and sheared anchor bolts at bearings	Not mentioned	Not clear	No
	Louisiana	Pavement growth	Backwall pushing on superstructure	Yes	Not mentioned
	Missouri	Failure of turned back wings at abutments	Not mentioned	Skew > 45°	Not mentioned

DESIGN AND CONSTRUCTION OF SKEWED STEEL I-GIRDER BRIDGES

AASHTO recommendations are followed by most responding state agencies, while some states have modifications on requirements that are tailored according to the status and research of their agency. Table 3 presents the skew limits larger than which a more refined method of analysis is required, along with the types of refined analysis. In addition to skew angle, the skew index—product of skew angle tangent and bridge width divided by bridge span length (AASHTO 2017, Article 4.6.3.3.2)—is commonly used to describe bridge skewness. A skew of 45° and skew index of 0.3 were most frequently mentioned by responding state agencies, so these parameters were chosen as reasonable targets to select bridges for field monitoring in the current research.

Table 3. Skew Thresholds and Corresponding Required Refined Methods of Analysis

Skew Threshold		State Agency	Type(s) of Analysis Required
Skew Angle	15°	Wisconsin	2D grid line analysis or 3D finite element analysis (FEA)
	20°	Louisiana	Grid line analysis or 3D FEA for determining deflections and camber
		Maryland	Grid line analysis to check secondary lateral forces for bracing and shear connector design
	25°	New Hampshire	Refined method of analysis
	30°	Michigan	Refined method of analysis
		Utah	Refined finite element or 2D grid analysis
	45°	Missouri	Consider additional 10% girder depth during preliminary design using line girder analysis
		New Hampshire	Finite element analysis
		Utah	3D FEA
		Wisconsin	3D FEA for bridge system
	60°	Illinois	Higher level of analysis to design bridge components, including cross-frames
Skew Index	0.2	Florida	Refined method of analysis; limit has been recommended to be increased to 0.3–0.4 with certain bridge geometric properties
	0.3	Pennsylvania	Refined analysis for non-curved bridges
	0.6	Florida	3D FEA
Not Specified		Colorado	Finite element analysis for all skewed bridges
		Louisiana	2D stiffness model or software with verified output, and validate with hand calculation, for all skewed bridges
		Minnesota	Plate and eccentric beam model or 3D FEA to design highly skewed steel I-girder bridges
		Pennsylvania	3D FEA using plate, shell, or solid elements to design severely skewed bridge; levels of analysis recommended in DOT design manual based on NCHRP Report 725

When determining the live load distribution factor (LLDF) for bridges with steel girders using approximate methods of analysis, the effect of skew is considered through an extra coefficient per Article 4.6.2.2 (AASHTO 2017). Corresponding AASHTO specifications are followed by most of the state agencies, along with a few additional reported considerations as recorded in Table 4. Differences in specifications from various state agencies indicate a need for improvement toward more uniform design guidelines.

Table 4. Additional Considerations for Determining Live Load Distribution Factors

State Agency	Application	Specification
Rhode Island DOT	General	Minimum LLDF used for exterior girder design = 0.6
Texas DOT	General	LLDF for moment or shear shall not be taken less than the number of lanes divided by the number of girders
Texas DOT	Exterior girder	Use LLDF of interior girder when slab cantilever is equal to or less than half the adjacent girder spacing; otherwise use lever rule with multiple presence factor of 1.0 for single lane

To achieve economical design and construction, most state agencies size exterior and interior girders the same. The field-monitoring effort of the current research aims to select bridges that follow this general practice. However, with the current AASHTO (2017) C6.10.1 suggestions recommending smaller lateral stress requirements for exterior girders than interior girders, such a design convention should be further evaluated. Design of exterior girders can be affected by the overhang width. IDOT encourages limiting the width of overhangs to 1 m (3.25 ft) or half the beam spacing. Typical reported minimum I-girder flange width could be 20% of girder depth, or 30/36 cm (12/14 in.), according to various survey responses. Utah DOT specifies that maximum I-girder flange width is 50% of girder depth, and Nebraska DOT requires girder flange width to be specified in 5 cm (2 in.) increments. Typical reported minimum I-girder flange thickness could be 2 cm (0.75 in.) or 2.5 cm (1 in.). Maximum flange thickness is 7.6 cm (3 in.), and maximum girder web thickness is stated to be 1.3 cm (0.5 in.) by Utah DOT. The typical girder flange width-to-thickness ratio ranges from 10 to 24, with an average of around 15.

Design of the concrete deck can also be complicated by skew, and deck placement as well as other phases of construction could be more critical when a bridge is highly skewed. Table 5 summarizes special requirements for deck design and placement, together with other construction concerns reported by state agencies. Wider bridges (a target of field monitoring in the current research) are prone to being constructed in stages, especially if there is a requirement to maintain traffic. When a bridge is constructed in two stages (of typically half the bridge), these may need to be considered in isolation under the effects of both construction and in-service live load. Even though the number of stages planned during construction is not skew-dependent according to most survey responses, the experiences of states with staged construction were still considered part of the background for the present study.

Table 5. Requirements for Deck Design and Constructability of Skewed Bridges

State Agency	Deck Design and Placement	Staged Construction and Construction Specifications
Colorado	Clear statement in contract is required for erected position of girders and fit condition for skew > 45°	Staged construction not used for skew > 45°
Delaware	Pour rates need to be watched carefully for skew > 45°	Rarely constructed in stages for skew > 45°
Illinois	For skew angle > 45°, or skew angle > 30°and deck pour width-to-span length ratio > 0.8, place and consolidate parallel to skew	Usually constructed in two stages, unless bridge is sufficiently wide to warrant a third stage
Louisiana	Perpendicular to girder reinforcement design at deck corners is specially considered for skew > 45°	None mentioned
Maryland	Deck placement not related to skew	Avoid staged construction for skew > 45°
Minnesota	Place perpendicular to skew; for skew > 45°, concrete overlay is required, and all deck forms are required to be constructed on beams; wearing course is required for a smooth ride during deck pour	Closure pour is required if deck differential deflection is larger than 8–10 cm (3–4 in.)
Nebraska	Empirical deck designed for skew > 45°; placed along skew	None mentioned
North Carolina	None mentioned	For skew > 45°, avoid staged construction, and girders required to be checked for potential overstress or uplift during erection
Pennsylvania	Deck is finished normal to centerline of bridge	Rarely constructed in stages for skew > 45°
Rhode Island	Add significantly more reinforcement at acute corners of deck for skew > 45°	None mentioned
Wisconsin	For skew > 20°, transverse joints between pours need to be “stepped”; slab placement and finishing equipment must be placed parallel to skew	None mentioned

DESIGN OF SECONDARY MEMBERS OF SKEWED STEEL I-GIRDER BRIDGES

Cross-frames play a significant role in constructability of bridges, and their function in carrying and transferring lateral load for skewed in-service bridges should also be considered. Table 6 presents the skew limit larger than which cross-frames should be designed rather than simply chosen from standardized sections. Cross-frames can play a significant role during the construction process, so they should be investigated for all stages of construction (as well as for the final in-service condition). Such structural response is of interest in the current research.

Table 6. Skew Threshold for Cross-Frame Explicit Design

Skew Angle Threshold	Design Requirements	Stage Agency
60°	Design as primary members through analysis	Illinois
20°	Design as load-carrying members	Pennsylvania
None	Always use standardized cross-frames for non-curved bridges	Wisconsin
Other (not skew related)	Design cross-frames as primary members if adjacent girders do not have similar stiffness	Utah

Cross-frames used in steel I-girder bridges are typically either X-shaped, K-shaped, or simply channels. Channel sections are generally used in bridges with rolled girders or shallow plate girders, while the other two types are more often used in bridges having deep plate girder cross-sections. Table 7 collects responses from state agencies on their preference for types of cross-frames in highly skewed bridges given other geometrical aspects of a bridge.

Cross-frames could be placed parallel to the skew line or perpendicular to the girder line—contiguous or staggered (discontinuous)—and the requirement for cross-frame layout varies with bridge skew. AASHTO Section 6.7.4 suggests cross-frames be placed perpendicular to the girders in a discontinuous manner when support lines are skewed more than 20° so that transverse stiffness of the bridge is reduced. It provides further guidance for engineers regarding cross-frame and diaphragm placement for skewed steel girder bridges. When cross-frames are placed perpendicular to girder lines, the first cross-frame near a support should be offset to alleviate a load path that would result in large transverse load to the support to reduce potential large cross-frame forces near the support and to generally eliminate potential unwanted stiffness near the support and in the cross-frames (Krupicka and Poellot 1993). Table 8 presents cross-frame layouts preferred by responding state agencies with associated skew limits. Most states mentioned that they prefer cross-frames to be placed staggered and perpendicular to the girder line, which was then the target for selecting bridges to be monitored in the current research.

Table 7. Preferred Types of Cross-Frames or Diaphragms

Preferred Type of Cross-Frame	State Agency	Usage
X-Shaped	Colorado	50% of bridges
	Florida	Non-curved bridges with girder spacing-to-depth ratio < 2.0 Illinois
	Iowa	90% of bridges
	Louisiana	Bridges with deep girders
	Michigan	Preferred
	Minnesota	80% of bridges
	North Carolina	Bridges with girder depth greater than 1.5 m (60 in.)
	New Hampshire	35% of bridges
	Pennsylvania	95% of bridges, when ratio of girder spacing to depth is not more than 1.0 for intermediate locations
	Utah	Narrow bridges with small girder spacing relative to girder depth
	Wisconsin	Bridges with girder web depth greater than 1.2 m (48 in.)
K-Shaped	Iowa	90% of bridges
	Colorado	50% of bridges
	Florida	More than 90% of bridges; more economic in design
	Illinois	End diaphragms—channels as top and bottom elements and L-sections as diagonal members
	Maryland	90% of bridges
	Michigan	Bridges with girder spacing larger than 3.8 m (12.5 ft) and all end diaphragms
	Missouri	70% of bridges
	North Dakota, Rhode Island, South Dakota	Required
	New Hampshire	65% of bridges
	Texas	Non-curved bridges regardless of skew
	Utah	Most plate girder bridges
Channel	Illinois	Interior diaphragms for bridges with girder depth less than or equal to 1 m (40 in.)
	Louisiana	Single-member diaphragms for shallow girders
	Minnesota	Bent plate diaphragms are used for rolled beams and plate girders less than 1 m (40 in.) deep
	North Carolina	Channels or W-sections for shallow girders (with girder web depth less than 1.2 m [49 in.])
	Utah, Wisconsin	Bridges with girder web depth less than 1.2 m (48 in.)

Table 8. Preferred Cross-Frame Layouts

Preferred Cross-Frame Layout	State Agency	Conditions for Preference
Parallel to Skew Line	Florida, Illinois, Maryland	Only if skew < 20°
	Nebraska	For skew < 25°
	Rhode Island	All bridges
	Utah	At supports or when skew < 20°
Contiguous Perpendicular to Girder Line	Florida, Maryland	For skew > 20°
	Iowa, North Dakota	All bridges
	Louisiana	Second most commonly used for highly skewed bridges
	Minnesota	70% of bridges, typically at interior locations
	Missouri	90% of bridges
	Pennsylvania	80% of bridges
Staggered Perpendicular to Girder Line	Colorado	Primarily used
	Illinois, Utah	For skew > 20°
	Louisiana	Most commonly used for highly skewed bridges
	Minnesota	30% of bridges, typically at end locations
	Missouri	10% of bridges
	Nevada, New Hampshire, North Carolina, South Dakota, Utah, Wisconsin	All bridges
	Pennsylvania	20% of bridges
Other	Louisiana	Minimize frame loading for skew > 45°
	Pennsylvania	Cross-frames need to be normal to girder tangents where one or both supports within a span are skewed > 20°

CHAPTER 3: FIELD-MONITORING CONFIGURATION

Field monitoring was conducted to evaluate the efficiency of current design practices for skewed steel I-girder bridge superstructures and to help make design suggestions for bridges of different geometries. In light of the general design and construction practices summarized in Chapter 2, and considering information from the agency survey, bridges skewed around or above 45° and designed with steel plate girders of substantial web height were investigated during the selection process for field monitoring. This chapter discusses the bridges selected for field monitoring, instrumentation of bridges, and methods of processing field measurements.

FIELD-MONITORING BRIDGES

Among bridges that were planned for construction within the first year of the project (2019), two relatively long bridges skewed around 45° were identified and chosen for field monitoring. These bridges are of similar geometry—one with stub abutments (Mattis-74, as presented in Figure 5) and the other with integral abutments (Mattis-57, as presented in Figure 6)—and in close vicinity of each other in Champaign, Illinois.

Table 9. Parameters for Mattis Avenue Bridges

Bridge	Mattis-74 (Figure 1)	Mattis-57
Number of Spans	Two-span continuous	Two-span continuous
Skew Angle	41°19’30”	45°00’00”
Abutment Type	Stub	Integral
Span Lengths	43.1 m, 51.9 m (141 ft 6-1/4 in., 170 ft 1-3/8 in.)	54.7 m, 53.6 m (179 ft 5-3/4 in., 175 ft 11-3/4 in.)
Bridge Width	25.6 m (84 ft)	16.7 m (54 ft 10 in.)
Skew Index	0.52, 0.43	0.35, 0.35
Number of Girders	12	8
Plate Girder Web Height	1.8 m (70 in.)	1.9 m (74 in.)
Cross-Frame Type	X-shaped	X-shaped
Cross-Frame Layout	Staggered, perpendicular to girder lines	Staggered, perpendicular to girder lines
Stages of Construction	3 stages (3rd stage is connection pour)	3 stages (3rd stage is connection pour)

Detailed information about the bridges is listed in Table 9. Mattis-74 is a stub abutment bridge with a skew angle of 41° and 12 I-girders of 1.8 m (70 in.) web height. Mattis-57 is an integral abutment bridge (IAB) with a skew angle of 45° and eight plate I-girders of 1.9 m (74 in.) web height. Both bridges are two-span continuous and have internal X-shaped cross-frames arranged perpendicular to the girder lines in a staggered configuration. The two bridges are expected to be under almost identical environmental conditions and experience similar traffic due to their proximity along the same route. As indicated by previous research (LaFave et al. 2021), steel bridge girder response could be complicated by the restraint of integral abutments. Also, general design practices reported by state agencies could be different for bridges with different types of abutments (e.g., regarding limits

on bridge length and width). Field monitoring and numerical simulations of Mattis-74 provide understanding of the effects of skew on bridge response without the complexity induced by superstructure-substructure interaction, while comparison between responses of the two bridges help separately evaluate effects from skew and substructure on skewed bridges.

FIELD INSTRUMENTATION

To better explain key performance issues in skewed bridges, as summarized from the agency survey, bridge monitoring was planned to capture behavior of skewed steel I-girder bridge superstructures under construction loading, traffic loading, and thermal effects. Strain variation at selected steel I-girders, critical cross-frames, and key concrete locations was measured with strain gauges. Rotations of select steel I-girders (measured with tiltmeters) and relative in-plane displacements between the bridge superstructure and substructure (measured with displacement transducers) were also collected. The field-monitoring campaign in this research project implemented sensing and data acquisition systems that are capable of capturing both short-term dynamic response and long-term response history.

Table 10. Parameters of Sensing and Data Acquisition Equipment

Sensor Type	Model	Range	Resolution	Accuracy
Weldable Strain Gauge (Figure 3-A)	Geokon 4150	3000 $\mu\varepsilon$	0.4 $\mu\varepsilon$	± 0.5% full scale
Embedded Strain Gauge (Figure 3-C)	Geokon 4200	3000 $\mu\varepsilon$	1.0 $\mu\varepsilon$	± 0.5% full scale
Tiltmeter (Figure 3-D)	Geokon 6350	10°	$\pm$0.05 mm/m (8 arc seconds)	$\pm$ 0.1% full scale
Crackmeter (Figure 3-E)	Geokon 4420	50 mm	0.025% full scale	$\pm$ 0.1% full scale
Multiplexer (Figure 4-A)	VWIRE305	8-channel dynamic vibrating wire analyzer		
Datalogger (Figure 4-A)	GRANITE9	Measurement and control data acquisition system		

Vibrating wire sensors from Geokon, Inc. (2022) were chosen to provide robust sensing capability for long-term measurements along with data acquisition systems from Campbell Scientific, Inc. (2022) that enable synchronized sampling rates up to 20 Hz. Parameters for the equipment are presented in Table 10. The main type of sensing equipment—a model 4150 strain gauge—has a 51 mm (2.0 in.) gauge length and is designed to measure strains in steel structures where space may be limited. These gauges can be installed quickly and easily by means of a capacitive discharge spot welder for long-term durable field monitoring, as presented in Figures 3-A and 3-B. The other type of strain gauge—a model 4200 gauge—can be secured to reinforcement and embedded to measure strain variation in concrete (Figure 3-C). Installation of tiltmeters (Figure 3-D) and crackmeters (Figure 3-E) will be elaborated further in this section. Temperature variation associated with other measurements is captured to further evaluate long-term temporal effects in and on bridge superstructures. All vibrating wire sensors have a built-in thermistor, and temperature data are read at a lower sampling rate with the strain, rotation, or displacement data on the same output channel. A Granite9 series datalogger is used for each bridge to collect, synchronize, and transmit data through modems. 8-channel dynamic vibrating wire analyzers (multiplexers) are used to connect sensing equipment to

the datalogger. Cables of the sensing equipment were connected to the data acquisition system (Figure 4-A) at the ends of the bridges, as presented in Figure 4-B. The systems were powered by solar panels for data collection and transfer (Figure 4-C).

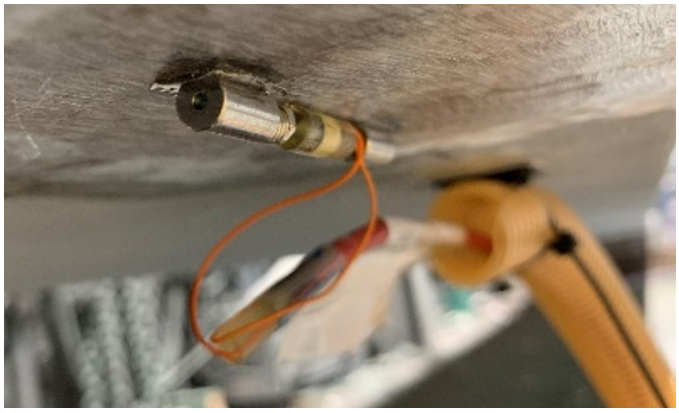

A. Weldable strain gauge (welded)

B. Weldable strain gauge (protected)

C. Concrete embedded strain gauge

D. Tiltmeter

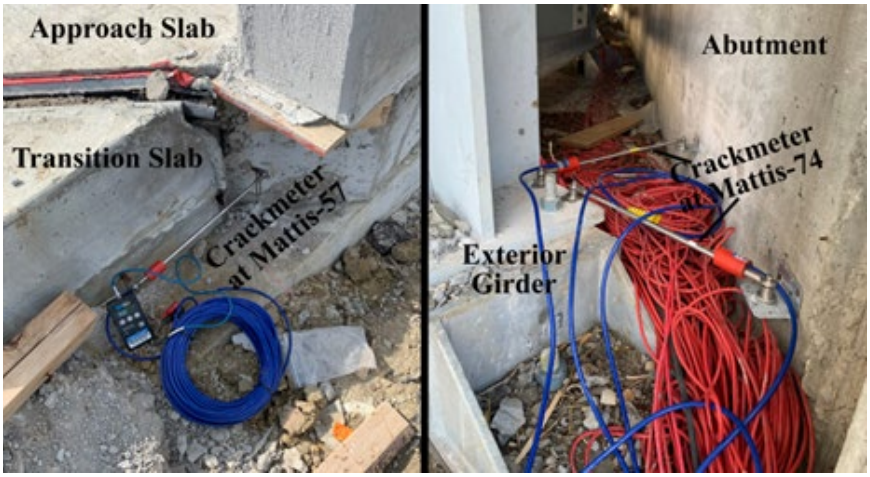

E. Crackmeter (displacement transsducer)

Figure 3. Photos. Sensing equipment.

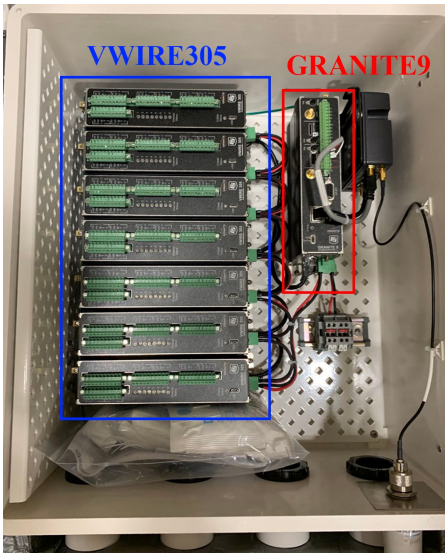

A. Data acquisition system

B. Control boxes

C. Control boxes

Figure 4. Photos. Data acquisition equipment.

Instrumentation of the bridges was planned for the selected bridges according to focal points of interest gleaned from the agency survey, findings of prior research, and the preliminary analysis, which will be presented in Chapter 5. Figures 5 and 6 show instrumentation plans for Mattis-74 and Mattis-57, respectively. The girders are labeled G1 through G12 for Mattis-74 and G1 through G8 for Mattis-57. The cross-frames are labeled CF1 through CF14 for Mattis-74 and CF1 through CF17 for Mattis-57. For both bridges, girder and cross-frame sections were instrumented where the largest compressive or tensile stresses were expected. For Mattis-57, there was additional focus on bridge acute and obtuse corners to observe behavior introduced by restraint at the integral abutments. The bridges were both constructed in three stages, where Stage I (approximately half of the bridge) was built and in service while Stage II was under construction. Stage III was then a closure pour between Stages I and II toward the end of construction. To allow the full instrumentation systems to be brought online all at once, and to capture behavior starting with the construction phase, the monitoring program focuses on the region of the bridges within the Stage I phase of construction. The concrete deck slab was placed in two phases (Phase 1 in the positive moment regions and Phase 2 in the negative moment region), as presented in Figures 5 and 6. Phases 1 and 2 were separated by six days, and Phase 1 deck placement was conducted in two parts during the same day—Phase 1.1 in the south span and Phase 1.2 in the north span for both bridges.

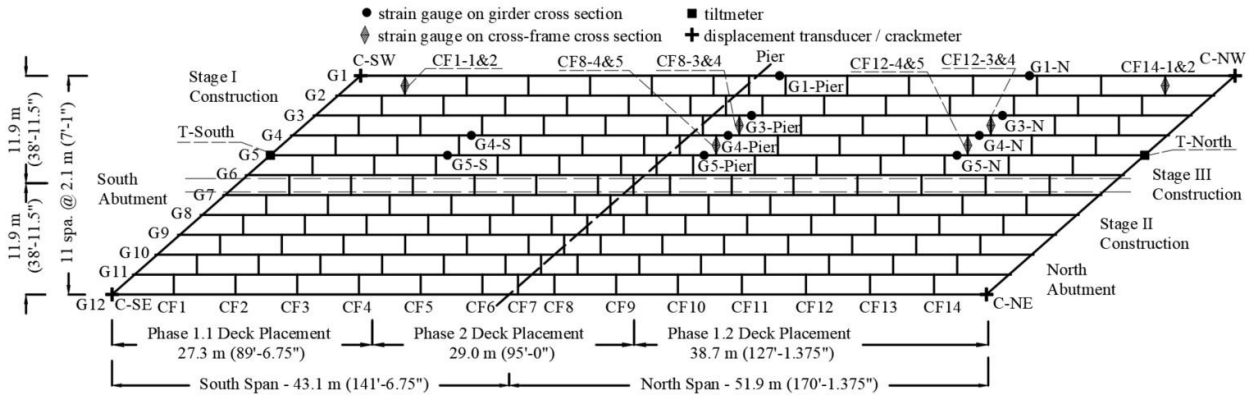

Figure 5. Plan view. Mattis-74 with instrument locations.

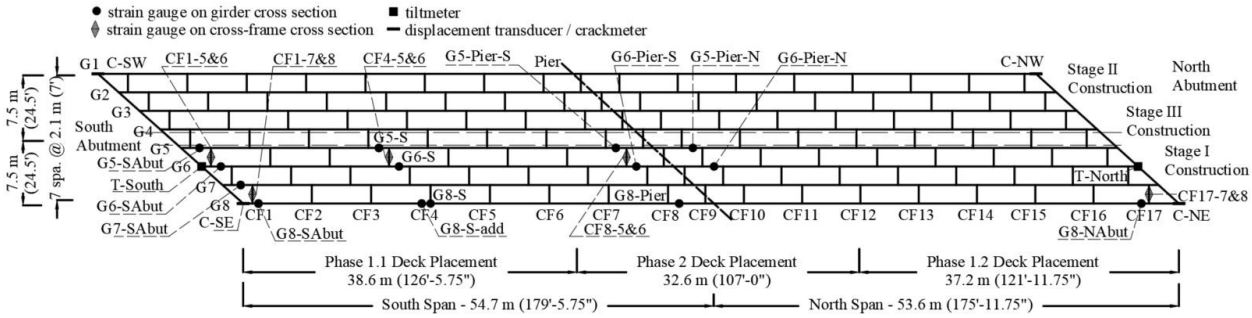

Figure 6. Plan view. Mattis-57 with instrument locations.

Girder cross-sections were either heavily instrumented—with eight strain gauges on the girder and one embedded gauge in the concrete deck, as presented in Figure 7-A—or lightly instrumented with fewer gauges. At a heavily instrumented section, eight strain gauges were spot-welded to the steel

girder and an embedded concrete strain gauge was tied to the reinforcing steel near mid-height of the deck before concrete placement. Interior girders under traffic lanes were chosen to be heavily instrumented. Exterior girders, as well as some other interior girders, were lightly instrumented. For Mattis-74, girder cross-sections G4-Pier, G5-Pier, G4-N, and G5-N are heavily instrumented, while for Mattis-57, girder cross-sections G6-SAbut, G6-Pier-S, and G6-Pier are heavily instrumented. Table 11 thoroughly records instrumentation on girder cross-sections for Mattis-74 and Mattis-57. Girder gauge locations were chosen between cross-frames to limit any disturbed region effects from connections, except for at G8-S-add on Mattis-57, where a comparison study was planned regarding the localized behavior near cross-frames. Gauge names are added to a girder cross-section or cross-frame name. For example, "G1-Pier-TE" represents the top flange east side strain gauge for Girder 1 near the center bridge pier.

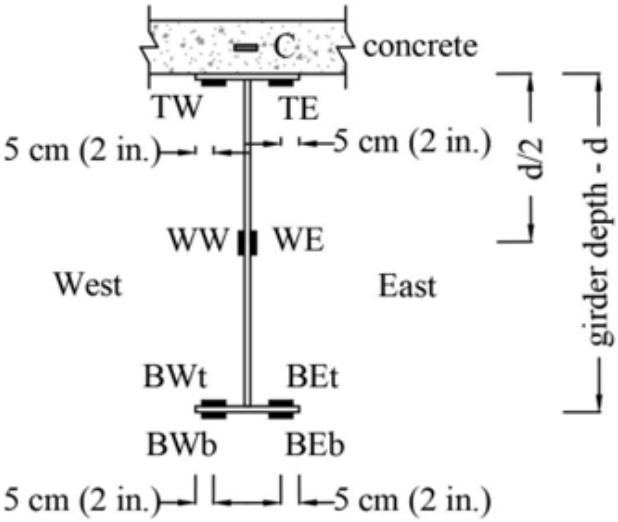

A. Girder cross-section

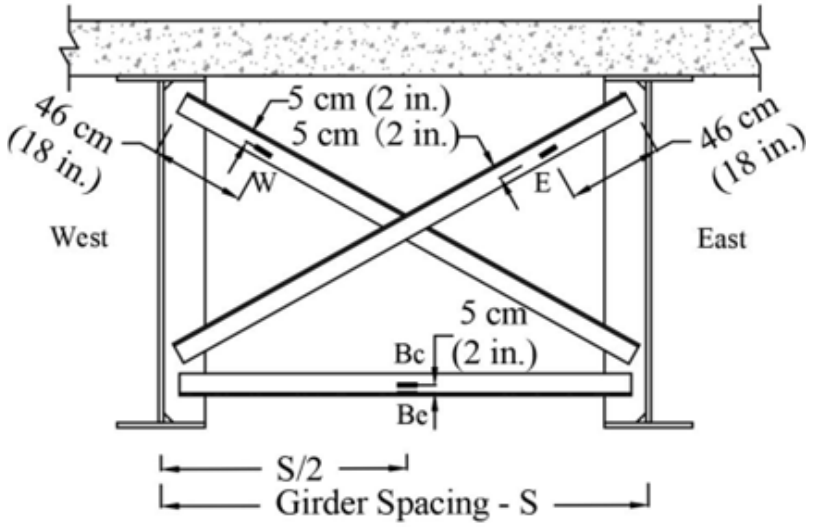

B Cross-frame

Figure 7. Schematic. Mattis-57 and Mattis-74 strain gauge locations.

Table 11. Strain Gauge Locations for Each Instrumented Girder Cross-Section

Bridge	Cross-Section	Strain Gauge Locations								
		C	TW	TE	WW	WE	BWt	BWb	BEt	BEb
Mattis-74	G4-S		√	√			√		√	
	G5-S		√	√				√		√
	G1-Pier		√	√				√		√
	G3-Pier		√	√				√		√
	G4-Pier	√	√	√	√	√		√	√	√
	G5-Pier	√	√	√	√	√		√	√	√
	G1-N		√	√				√		√
	G3-N		√	√				√		√
	G4-N	√	√	√	√	√		√	√	√
	G5-N	√	√	√	√	√		√	√	√
Mattis-57	G5-SAbut		√	√				√		√
	G6-SAbut	√	√	√	√	√		√	√	√
	G7-SAbut		√	√				√		√
	G8-SAbut		√	√				√		√
	G5-S		√	√				√		√
	G6-S	√	√	√	√	√		√	√	√
	G8-S		√	√				√		√
	G8-S-add			√						√
	G5-Pier-S		√	√				√		√
	G5-Pier-N			√						√
	G6-Pier-S	√	√	√	√	√		√	√	√
	G6-Pier-N		√	√			√		√	
	G8-Pier		√	√				√		√
	G8-NAbut		√	√				√		√

Cross-frames near heavily instrumented girder cross-sections and close to bridge corners were monitored to understand the load path at those locations. Diagonal and bottom members of the cross-frames are all L100 × 100 × 10 mm (L4 × 4 × 3/8 in.). Three strain gauges were typically installed at an instrumented cross-frame location: at the west top portion of one diagonal angle (W), at the east top portion of the other diagonal angle (E), and at mid-length of the bottom chord angle on the concentric leg (Bc) (Figure 7-B). For location CF1-1&2 on Mattis-74, an additional strain gauge was placed at mid-length of the bottom chord angle on the eccentric leg—named CF1-1&2-Be—to study localized behavior of cross-frame members.

Tiltmeters ("T") were mounted at the two ends of a critical girder, G5 for Mattis-74 and G6 of Mattis-57, to measure girder end rotations. The tiltmeters were mounted mid-height of end bearing stiffeners of Mattis-74-G5 and on an abutment of Mattis-57 very close to mid-height of G6. Prior research observed that the relative rotation between abutment and girder at the ends of IABs is negligible (LaFave et al. 2021). Linear displacement transducers (crackmeters, "C") were mounted at the four corners (C-SW, C-NW, C-SE, and C-NE) of both bridges to measure relative movement between the bridge superstructure and substructure. Crackmeters were installed both along and perpendicular to the girder line for the stub abutment bridge (Mattis-74, Figure 5), between the abutment and girder bottom flange (at bearing level), and only along the girder line for the IAB (Mattis-57, Figure 6) between the approach slab and transition slab (approach-transition at deck level).

FIELD DATA PROCESSING SCHEME

Normal strain induced at a gauge location (ε_{gauge}) of a girder cross-section can be decomposed into components related to axial force (ε_P), strong-axis bending moment (ε_{M_x}), lateral bending moment (ε_{M_l}), and local plate bending (ε_{Local}), as presented in Figure 8. As described below, lateral bending is associated with an individual flange—top ($\varepsilon_{M_{lt}}$) or bottom ($\varepsilon_{M_{lb}}$). This section explains the method to calculate global and local strain components from field strain measurements, which has been used to evaluate field monitoring and numerical simulation results in this project.

$$\varepsilon_{gauge} = \varepsilon_P + \varepsilon_{M_x} + \varepsilon_{M_l} + \varepsilon_{Local}$$

Figure 8. Equation. Stress decomposition.

Axial force (*P*), strong-axis bending moment (M_x), and weak-axis (lateral) bending moments (M_l) are global actions contributing to normal strain for bridge girders under live and dead load, as presented in Figure 9 (where plane section behavior is assumed). ε_P is a uniform effect through the depth at a girder cross-section, and cross-sectional strong-axis bending curvature (K_x) is not affected by this uniform axial strain. The elastic centroid of the cross-section can be calculated for either a steel girder (when the bridge is analyzed under deck placement) or a composite girder (when studying live load after the bridge is in service). For an I-girder that is symmetric about its *y*-axis (Figure 9), ε_{M_x} at a certain distance *y* from the *x*-axis elastic centroid can be calculated for any point of interest in the section by Figure 10, where *E* is the elastic modulus of steel and I_x is $I_{tr,x}$ (moment of inertia of the uncracked transformed section) for composite girders or I_s (moment of inertia of the steel I-section) for non-composite girder cross-sections. When a composite section is considered, the effective overhanging flange width of the concrete deck slab on one side of a girder is taken as half the distance to the adjacent girder for an interior condition and the edge-of-slab dimension for an exterior condition. K_x can be determined through the calculation method presented in the following paragraphs or estimated by conducting linear regression using *y*-axis strain measurements from both the steel I-section and concrete deck. The two methods of evaluating K_x were cross-validated, based on which the accuracy of the proposed strain decomposition approach was verified.

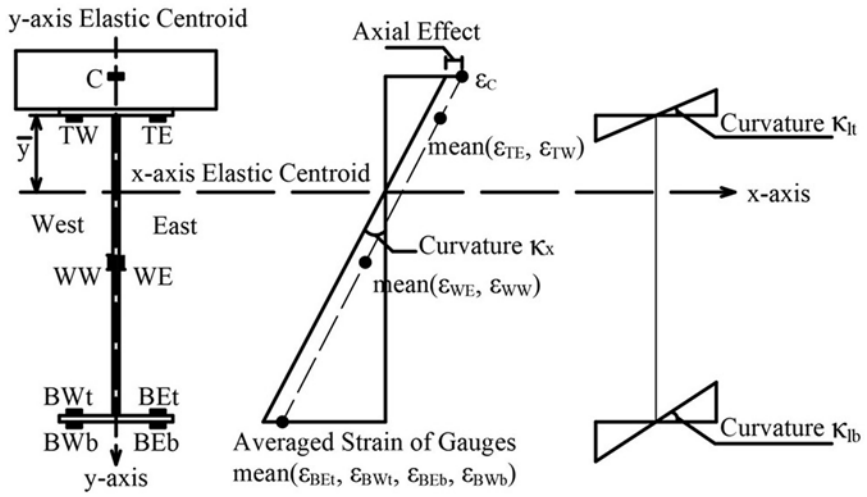

Figure 9. Schematic. Strong-axis and weak-axis flexure of an I-girder.

$$\varepsilon_{M_x} = \frac{M_x}{EI_x} y = \mathrm{K}_x y$$

Figure 10. Equation. Calculation of strain induced by strong-axis bending.

Normal strain induced by lateral bending of the girder top flange $\varepsilon_{M_{lt}}$ (and bottom flange $\varepsilon_{M_{lb}}$) at x_t (and x_b) away from the weak-axis elastic centroid (girder y-axis) can be calculated according to Figure 11 (and Figure 12). M_{lt} and M_{lb} are lateral bending moments acting on the top and bottom flanges, respectively, which include both global weak-axis bending moment and cross-flange bending due to restraint of warping. I_{yt} and I_{yb} are the weak-axis moments of inertia of the plate girder top and bottom flanges, respectively, and K_{lt} and K_{lb} are the weak-axis bending curvatures of the girder top and bottom flanges, respectively, as presented in Figure 9.

$$\varepsilon_{M_{lt}} = \frac{M_{lt}}{EI_{yt}} x_t = \mathrm{K}_{lt} x_t$$

Figure 11. Equation. Calculation of strain induced by top flange lateral bending.

$$\varepsilon_{M_{lb}} = \frac{M_{lb}}{EI_{yb}} x_b = \mathrm{K}_{lb} x_b$$

Figure 12. Equation. Calculation of strain induced by bottom flange lateral bending

Elaborating on Figure 8, the normal strain at each bottom flange gauge location of a heavily instrumented girder cross-section can be expressed in Figures 13 and 14. These equations correspond to the east side. Similar equations for the west side are not shown for brevity, but equations for both the east and west sides are presented together in matrix form in Figure 17. With symmetric placement of bottom flange gauges about the *y*-axis, averaging Figures 13 and 14 yields Figure 15, which corresponds to the strain at mid-thickness of the girder bottom flange on the east side

(without considering responses due to flange plate local bending). Similarly, Figure 16 illustrates the normal strain component at the bottom face of the girder top flange on the east side. Figures 15 and 16 (for the east side) can then be formalized into matrix form, along with the similar equations for the west side, as presented in Figure 17, where the left-side vector contains measured strains and the right-side vector contains unknown axial strain and curvature values associated with the decomposed effects on the section. With a set of measured strains and the inverted coefficient matrix, which contains known geometric parameters associated with gauge locations, the unknown axial strain and curvatures can be calculated.

$$\varepsilon_{BEb} = \varepsilon_P + \mathrm{K}_x y_{BEb} + \mathrm{K}_{lb} x_{BEb} + \varepsilon_{east}$$

Figure 13. Equation. Decomposition of strain at the bottom of the east side of bottom flange.

$$\varepsilon_{BEt} = \varepsilon_P + \mathrm{K}_x y_{BEt} + \mathrm{K}_{lt} x_{BEt} - \varepsilon_{east}$$

Figure 14. Equation. Decomposition of strain at the top of the east side of bottom flange.

$$\varepsilon_{BE} = \varepsilon_P + \mathrm{K}_x y_{BE} + \mathrm{K}_{lb} x_{BE}$$

Figure 15. Equation. Decomposition of strain at the east side of bottom flange.

$$\varepsilon_{TE} = \varepsilon_P + \mathrm{K}_x y_{TE} + \mathrm{K}_{lt} x_{TE}$$

Figure 16. Equation. Decomposition of strain at the east side of top flange.

$$\begin{Bmatrix} \varepsilon_{TE} \\ \varepsilon_{TW} \\ \varepsilon_{BE} \\ \varepsilon_{BW} \end{Bmatrix} = \begin{bmatrix} 1 & y_{TE} & x_{TE} & 0 \\ 1 & y_{TW} & x_{TW} & 0 \\ 1 & y_{BE} & 0 & x_{BE} \\ 1 & y_{BW} & 0 & x_{BW} \end{bmatrix} \begin{Bmatrix} \varepsilon_P \\ \mathrm{K}_x \\ \mathrm{K}_{lt} \\ \mathrm{K}_{lb} \end{Bmatrix}$$

Figure 17. Equation. Matrix representation of strain decomposition.

For a lightly instrumented girder cross-section where the girder bottom flange was only measured on one surface—the bottom surface (BEb and BWb) or top surface (BEt and BWt)—Figure 15 is directly associated with a gauge location on the flange surface (Figures 13 and 14) and not the flange mid-thickness strain. When a girder cross-section is lightly instrumented on only one side of the I-girder, the east side (TE and BE) or west side (TW and BW), ε_P and K_x can be calculated with a reduced matrix form (Figure 18), considering only geometric information of the strain gauges with respect to *x*-axis elastic centroid. This condition, however, can produce inaccurate results for strong-axis bending values if large lateral bending exists either in the top or bottom flange. In addition, lateral bending behavior cannot be analyzed for either the girder top or bottom flange in this scenario. In all cases (Figures 17 and 18), decomposed strain due to strong-axis and weak-axis bending moment at each

strain gauge location can then be calculated according to the linear relationships indicated in Figures 10 through 12. A previous research project that conducted large-scale field testing on curved I-girder bridges used a similar approach to decompose girder cross-sectional behavior (Greimann et al. 2014).

$$\begin{Bmatrix} \varepsilon_T \\ \varepsilon_B \end{Bmatrix} = \begin{bmatrix} 1 & y_T \\ 1 & y_B \end{bmatrix} \begin{Bmatrix} \varepsilon_P \\ \mathrm{K}_x \end{Bmatrix}$$

Figure 18. Equation. Matrix representation of strain decomposition.

For heavily instrumented girder locations, subtracting Figure 14 from Figure 13 evaluates strain due to flange plate local bending at the east side (Figure 19), and a similar expression can be derived for the west side (Figure 20). Strain components at girder web gauges can be expressed as Figures 22 and 23, where strain due to out-of-plane behavior of a girder web (ε_{web}) results from a combination of global weak-axis bending and web plate local bending. ε_{web} can then be calculated using Figure 24. Bridge superstructure components are, in general, expected to behave elastically under service loads (dead, thermal, and traffic), so the decomposed strain can then be converted to a decomposed stress by simply multiplying the strain by the elastic modulus for either steel or concrete.

$$\varepsilon_{east} = \frac{\varepsilon_{BEb} - \varepsilon_{BEt} - \mathrm{K}_x(y_{BEb} - y_{BEt})}{2}$$

Figure 19. Equation. Calculation of flange plate local bending on the east side.

$$\varepsilon_{west} = \frac{\varepsilon_{BWb} - \varepsilon_{BWt} - \mathrm{K}_x(y_{BWb} - y_{BWt})}{2}$$

Figure 20. Equation. Calculation of flange plate local bending on the west side.

$$\varepsilon_{BE} = \varepsilon_P + \mathrm{K}_x y_{BE} + \mathrm{K}_{lb} x_{BE}$$

Figure 21. Equation. Decomposition of strain at the east side of bottom flange.

$$\varepsilon_{WE} = \varepsilon_P + \mathrm{K}_x y_{WE} + \varepsilon_{web}$$

Figure 22. Equation. Decomposition of strain at the east side of web.

$$\varepsilon_{WW} = \varepsilon_P + \mathrm{K}_x y_{WW} - \varepsilon_{web}$$

Figure 23. Equation. Decomposition of strain at the west side of web.

$$\varepsilon_{web} = \frac{\varepsilon_{WE} - \varepsilon_{WW}}{2}$$

Figure 24. Equation. Calculation of web local bending.

When analyzing field measurements and validating model accuracy, strain measurements and stresses from numerical simulation were taken at and analyzed regarding gauge locations. For a fully instrumented girder cross-section where both surfaces of bottom flange were instrumented, strong-axis bending stress is evaluated and compared at the more extreme fiber for the bottom flange—at the bottom surface. When numerical simulation results were used for parametric studies, stress readings were extracted from flange edge elements, and decomposed stress was calculated at the flange tip to evaluate maximum strong-axis bending and lateral bending of a girder cross-section.

CHAPTER 4: NUMERICAL SIMULATION APPROACH

Three-dimensional finite element analysis was conducted using ABAQUS (2017) to enhance understanding of field response and to strengthen evaluation of bridge behavior through parametric studies. This chapter discusses validated numerical simulation methods, including modeling of bridge structural components and connections, representation of boundary conditions, and loading and data extraction approaches. Numerical simulation methods for bridges under construction (pre-composite with only steel I-girders and cross-frames) and while in service (composite) are presented.

BRIDGE COMPONENTS AND CONNECTIONS

Figure 25 presents an overview of the ABAQUS numerical model for Mattis-74 under construction, which is a typical 3D model of a pre-composite stub abutment bridge. Some elements are hidden for clarity in the detailed views in the figure. Numerical simulation of in-service bridges includes a concrete deck instead of the wooden formwork (false deck). Representation of the connection between steel I-girders and the deck (in service) or false deck (construction) varies between computational modeling of the two conditions, which will be elaborated on in this section. In addition, numerical simulation methods for integral abutment bridges (IABs) were mostly identical to those of stub abutment bridges except for the representation of the bridge end boundary conditions, which will be further illustrated in later sections. All abovementioned instances were meshed with a typical element size of 13 cm (5 in.), which was sufficiently accurate based on a sensitivity study using detailed meshes up to 2.5 cm (1 in.).

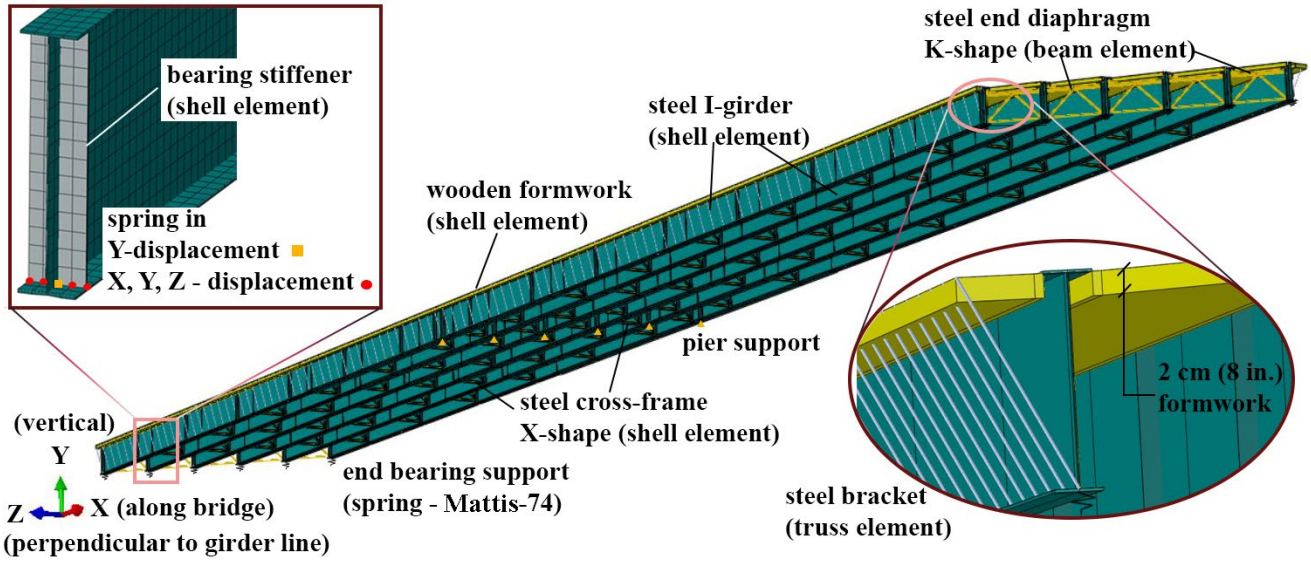

Figure 25. Illustration. Overall view of typical bridge model in ABAQUS—Mattis-74 under construction.

Steel I-girders, a concrete slab for bridge in-service conditions (or a wooden formwork for bridge construction conditions), steel cross-frames, and steel stiffeners were all explicitly modeled with 3D 4-node reduced integration shell elements (S4R), and steel end diaphragms in skewed stub abutment bridges were modeled with 3D 2-node linear beam elements (B31). Global coordinates are defined (Figure 25), where *X* is along the girder line, *Y* is the vertical direction, and *Z* is perpendicular to the girder line. The corresponding displacement degrees of freedom (dofs) are U_X, U_Y, and U_Z, and the corresponding rotational dofs are θ_X, θ_Y, and θ_Z. The bridge was considered to behave elastically under dead load and traffic, so linear elastic material properties were used to model steel and concrete elements.

Girders were defined as continuous over their full length, with tie-constraints for all dofs at splices and changes in cross-section. Bent plates, transverse stiffeners, and bearing stiffeners were all modeled as simple rectangular plates. They were connected to girder webs and flanges with tie-constraints in all dofs along all contacting edges. Connections between the two diagonal angle members of cross-frames were simplified as tie-constraints in all dofs at the region of the connection plate, and connections of cross-frames and transverse stiffeners were simplified as tie-constraints in all dofs over the bolted area. Cross-frame angle end connections were defined to the connected leg of the angle, accounting for realistic eccentric loading. These connection-related simplifications were sufficient to reasonably capture global cross-frame behavior and load transfer between I-girders through the cross-frames.

Haunches were modeled to represent the concrete slab for in-service bridges, and composite behavior was defined with tie-constraints connecting nodes of the haunches and steel girder top flanges in all six dofs. To validate numerical simulation methods regarding bridge in-service conditions, the bridge sidewalk (Mattis-74) and parapet (Mattis-57) were modeled as structural components fully connected to the concrete deck. Including these parts improved simulation accuracy, especially for exterior girders, which was also implied in prior research (White and Jamath 2020). To better control parameters, on the other hand, these less significant structural parts were not considered during parametric studies. When considering the bridge during the deck placement process, girder top flanges were connected with wooden formwork as a platform to support and distribute wet concrete dead load during deck placement. Figure 26 presents a schematic (cross-frames not shown for clarity) and field photos from the instrumented Mattis Avenue bridges.

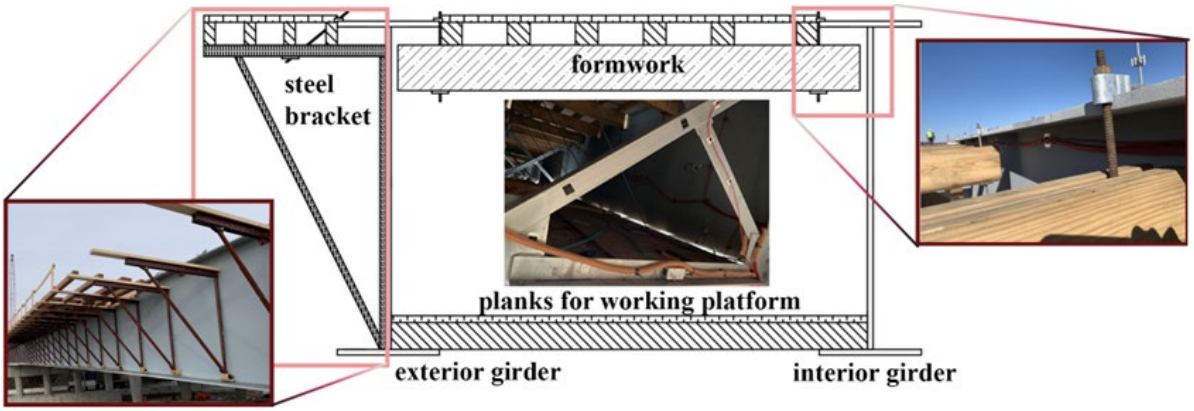

Figure 26. Illustration. Bridge formwork.

Parametric studies were conducted to acquire reasonable simplifications for modeling the formwork that efficiently capture girder and cross-frame behavior. As a result, the formwork was modeled as 20 cm (8 in.) thick shell elements with a material with low elastic modulus of 138 MPa (20 ksi), as presented in Figure 25. A similar assumption for modeling wooden formwork with low-stiffness material was used in previous research (Azizinamini et al. 2003). The overhang portion of the formwork was supported by steel brackets in the field to transfer load to both top flange and bottom flange, as illustrated in Figure 26. Related connections have been described in detail by prior research (Clifton and Bayrak 2008). The brackets were modeled by truss elements connecting the edge of the formwork to the girder bottom flange-web junction. Brackets were spaced regularly at 0.9 m (3 ft) apart in the models along the bridge length to approximate the field condition, which had some variability. Edges of formwork and girder top flanges were tied with all displacement dofs, and steel brackets were also connected to the outer edge of formwork (on the top) and along the girder bottom flange-web junction (on the bottom) with all displacement dofs. Planks spanning between girder bottom flanges provided a working platform during construction and were deemed to play an insignificant role in load transfer, so they were not included in the model.

BRIDGE BOUNDARY CONDITIONS

As mentioned in the prior section, the only difference in numerical simulation methods for stub abutment and integral abutment bridges lies in representation of bridge end supports. Boundary conditions at the end of a stub abutment bridge are unchanged during construction and after the bridge is in service, whereas those for an IAB differ because of the existence of abutments after deck placement. This section separately describes modeling of end boundary conditions of both types of bridges and ways to capture constraints at inner supports of typical multi-span continuous bridges, such as the middle pier support of the Mattis Avenue bridges (selected for field monitoring).

End Support of Stub Abutment Bridge

Bearings at the two end supports of Mattis-74 are Type I 13-d elastomeric bearings designed according to the IDOT *Bridge Manual* (2012), which is typical for stub abutment bridges in Illinois. The superstructure of these bridges is significantly stiffer than the bearing support and, therefore, was not explicitly modeled in this research focusing on capturing bridge superstructure behavior. Girder end boundary conditions of stub abutment bridges were represented by simplified bearing properties connected to a rigid substructure. The detailed view in Figure 25 presents the nodes across the girder bottom flange width at a bearing stiffener where the bearing properties are defined in displacement dofs. At a bearing stiffener, an expansion bearing is represented with linear springs in the *X*-, *Y*-, and *Z*-directions at the web-flange intersection node, and linear springs in the *Y*-direction at other nodes across the bottom flange width, as presented in Figure 25.

Springs in displacement dofs were defined to represent the bearing support, with their stiffnesses determined by recommendations from previous research. Parametric studies proved that defining rotational springs was redundant with the abovementioned modeling methods. Rotational dofs were therefore not restrained for representation of stub abutment bridge boundary conditions at bearings. Shear stiffness (K_H) and compressive stiffness (K_V) of the elastomeric bearings were calculated following Figures 27 and 28, respectively (Barbaros and Sevket 2017). In the equations, *G* is the shear

modulus of the elastomer, *A* is the area of an individual elastomer pad, *I* is the moment of inertia of the group of the elastomer pads, and *h* is the total height of the elastomer pads. *E* is the compressive elastic modulus of the elastomer, calculated with either Figure 29 or Figure 30, where *S* is the shape factor of the elastomer, E_0 is Young's modulus of the elastomer, and ϕ is empirically determined material property of the elastomer, as defined in Chapter 8 of *Engineering with Rubber: How to Design Rubber Components* (Barbaros and Sevket 2017; Gent 2012).

$$K_H = \frac{GA}{h}$$

Figure 27. Equation. Calculation of shear stiffness of elastomeric bearing.

$$K_V = \frac{EA}{h}$$

Figure 28. Equation. Calculation of compressive stiffness of elastomeric bearing.

$$E = E_0(1 + 2\phi S^2)$$

Figure 29. Equation. Calculation of compressive elastic modulus of elastomer (method 1).

$$E = 4.8GS^2$$

Figure 30. Equation. Calculation of compressive elastic modulus of elastomer (method 2).

Using Mattis-74 as an example, the elastomeric bearings have six layers of 1.6 cm (5/8 in.) elastomer pads and five layers of 0.4 cm (3/16 in.) steel plates. The width of the elastomeric bearings is 33 cm (13 in.), and the length of the bearings is 51 cm (20 in.), which corresponds to bearing Type I 13-d with a shape factor of 6.30 (IDOT 2012). Shear modulus was taken as 0.8 MPa (115 psi), Young's modulus was considered 3.2 MPa (460 psi), and material compressibility coefficient was determined to be 0.64 (Gent 2012). Shear stiffness and compressive stiffness were calculated as 721 N/m (6,380 lb/in.) and 1.86e^{5}N/m (1.65e^6 lb/in.), respectively, using Figures 27 to 30, which matched with the range of values observed by previous research studying Type I elastomeric bearing (Steelman et al. 2013). Steelman et al. (2018) studied retainer properties of elastomeric bearings through laboratory testing and concluded that retainer stiffness under small displacement could be taken as the bearing stiffness in the horizontal direction. Spring stiffness of 7.9e^3 N/m (7e^4 lb/in.) for expansion bearings in the bridge horizontal direction was therefore used in the current research.

Rotational stiffnesses (K_θ) of elastomeric bearings can be calculated using either Figure 31 or section 12.7.3 of Australia Standards (2004), which yield similar results. Rotational stiffness of elastomeric bearings on Mattis-74 using Figure 31 was 4.9e^6 N/m/rad (4.3e^7 lb/in./rad), and the calculated result using the Australia Standards (2004) was 3.9e^6 N/m/rad (3e^7 lb/in./rad). Previous research (Ishii et al. 2016; Mitoulis 2015; Reis et al. 2020; Roeder et al. 1987) reported rotational stiffness of elastomeric bearing of various dimensions ranging from 1.2e^6 N/m/rad (1.1e^7 lb/in./rad) to 2.9e^7 N/m/rad (2.6e^8

lb/in./rad). However, restraints in rotational dofs were not defined for modeling end boundary conditions of stub abutment bridges, as previously mentioned.

$$K_\theta = \frac{1.6(0.5EI)}{h}$$

Figure 31. Equation. Calculation of rotational stiffness of elastomeric bearing.

End Support of Pre-Composite Integral Abutment Bridge

Before deck and integral abutment placement, girder ends of IABs are connected directly to the pile cap with a bearing plate and a pair of anchor bolts at the bottom flange, as presented in Figure 32-A. The steel bearing plate that connected the girder bottom flange to the pile cap before concrete placement was represented as a set of five 5 cm (2 in.) long compression-only truss elements with a circular cross-section at an area of 6.5 cm^2 (1 $in.^2$) along the bottom flange at the end bearing stiffeners. The struts were pinned (restrained in all displacement dofs) both to the girder bottom flange and to the ground, as illustrated in Figure 32-B. Two beam elements with a circular cross-section and a 2.5 cm (1 in.) diameter were modeled to simulate the contribution from the pair of bolts in preventing girder uplift and in-plane movements. The effective bolt length was taken as 15 cm (6 in.)—the distance between the top of the girder bottom flange and the concrete surface. The beam members were fixed to the ground (restrained in all dofs), and they were pinned (restrained in all displacement dofs) to the girder bottom flange at mid-width of the flange plate on both sides. Both the truss and the beam elements were modeled with linear elastic steel material. The beam elements were modeled with both tension and compression capacity.

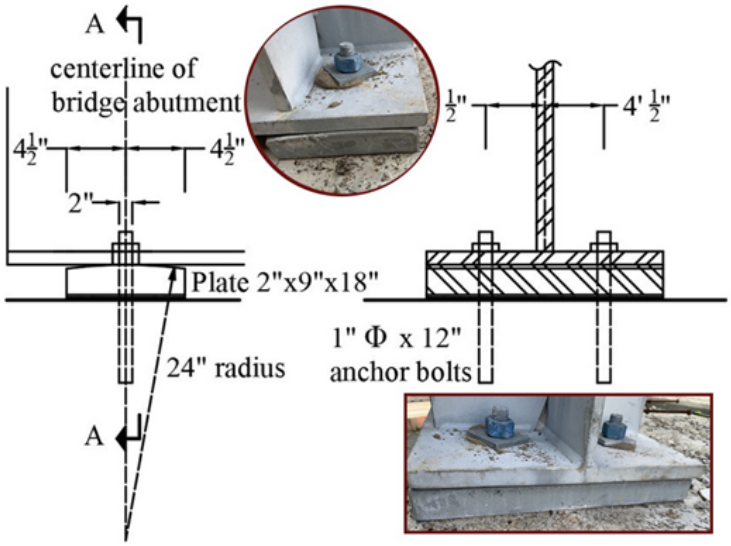

A. Field photos and drawing details

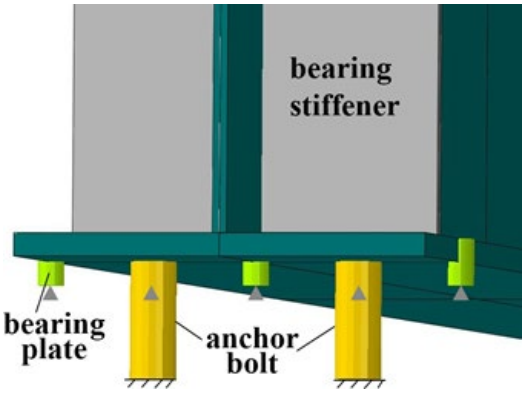

B. Representation of ABAQUS simulation

Figure 32. Illustration. Girder end support condition before deck placement of Mattis-57.

End Support of In-Service Integral Abutment Bridge

Abutments for IABs are typically cast together with the bridge concrete deck. Therefore, integral abutment and abutment cap were modeled as concrete shell elements (S4R), meshed with the same element size of 13 cm (5 in.) as other instances. Rigid connections between the abutment and superstructure (deck and girders) were represented with tie constraints in all dofs, as prior research indicated no relative movement at these intersections (LaFave et al. 2016). Backfill soil, piles, and surrounding soil all contributed to interaction between the abutment and ground. Figure 33 presents the computational modeling features for the integral abutment of Mattis-57, which served as a representative illustration for numerical simulation of the end boundary condition of IABs.

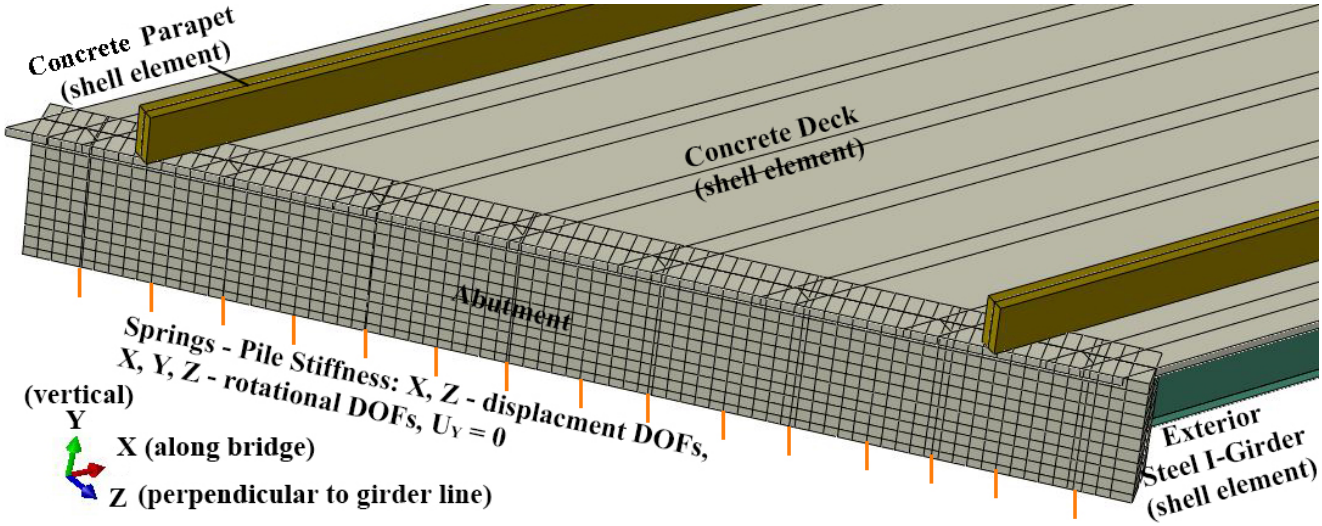

Figure 33. Illustration. Typical integral abutment in ABAQUS—Mattis-57.

Backfill soil friction and passive pressure (not considering at-rest or active pressure) were represented as springs in displacement dofs along and perpendicular to the abutments, respectively. Granular soil was used to calculate backfill properties for Mattis-57, which is a typical backfill material for bridges

in Illinois (LaFave et al. 2016). Loose sand with a unit weight of 20k N/m^3 (125 pcf) and an internal friction angle of 30° was used. Elastic perfectly plastic springs were modeled for the backfill, with maximum soil resistance achieved at 2.5 cm (1 in.) deformation (Clough and Duncan 1990; Shamsabadi et al. 2007). The backfill springs were discretely defined along the length and height of the abutment every 0.3 m (1 ft), as shown in Figure 33. However, a parametric study found that representing soil pressure as resultant stiffness (at two-thirds the depth of the abutment) accurately captures the triangular load distribution, which was also mentioned in Olson et al. (2013).

Contributions from piles under integral abutments were modeled as lumped springs, at and between girders under the abutment, in all rotational dofs and *X*- and *Z*-direction displacement dofs. Displacement dof in the *Y*-direction was restrained (set to zero). Stiffnesses of the springs were determined through analysis of piles individually, restrained in all displacement and rotational dofs at the bottom and surrounded by soil springs along the height. The soil was modeled using nonlinear springs in the *X*- and *Z*-directions of displacement dofs, spaced every 0.3 m (1 ft) for the first 4.5 m (15 ft) and every 1.5 m (5 ft) for the remaining deeper pile length. Uniform stiff clay was considered the surrounding soil for Mattis-57, which is predominant for the bridge (stated in the boring logs) and representative of many bridges in Illinois. Soil stiffness was calculated through p-y curves developed using LPILE, the result of which was validated through hand calculations using established procedures (Reese and Welch 1975). Both computational and analytical methods were developed regarding stiff clay. The undrained shear strength at different pile depths used to generate p-y curves was obtained from unconfined compressive strength provided in boring logs. The simplified approach to represent each pile with a set of lumped springs was validated with good accuracy when compared with explicit inclusion of piles and surrounding soil springs in the model.

Middle Support of Continuous-Span Bridge

Methods for modeling bridge middle pier support were developed through a few iterations. For analyzing a bridge superstructure under live load and concrete dead load, the middle support can be treated predominantly as restrained support with respect to a rigid substructure (ground), as a simplified representation (reported in Zhou et al. 2022). When studying bridge behavior during deck placement, the displacement dofs in the *X*-, *Y*-, and *Z*-directions were restrained across the bottom flange width at the middle (pier) bearing stiffener. When studying the in-service bridge behavior under live load, the vertical (*Y*-direction) displacement dofs (U_Y) were still restrained at nodes across the width of the bottom flange at the bearing stiffener, while both vertical and along bridge displacement dofs (U_Y and U_Z) were restrained at the girder web-flange intersection node for the pier support.

The abovementioned simplified representation of bridge middle support yielded satisfying comparisons between numerical simulation results and field measurements, considering bridges under concrete dead load and traffic live load. However, the modeling assumptions could be improved when considering bridges under thermal load. A further developed numerical simulation method considers the stiffness of pier and the connection between the I-girder bottom flange and pier. The method for intermediate support of continuous-span bridges is presented in Figure 34, taking girder-pier connection geometries of Mattis-74 as an example.

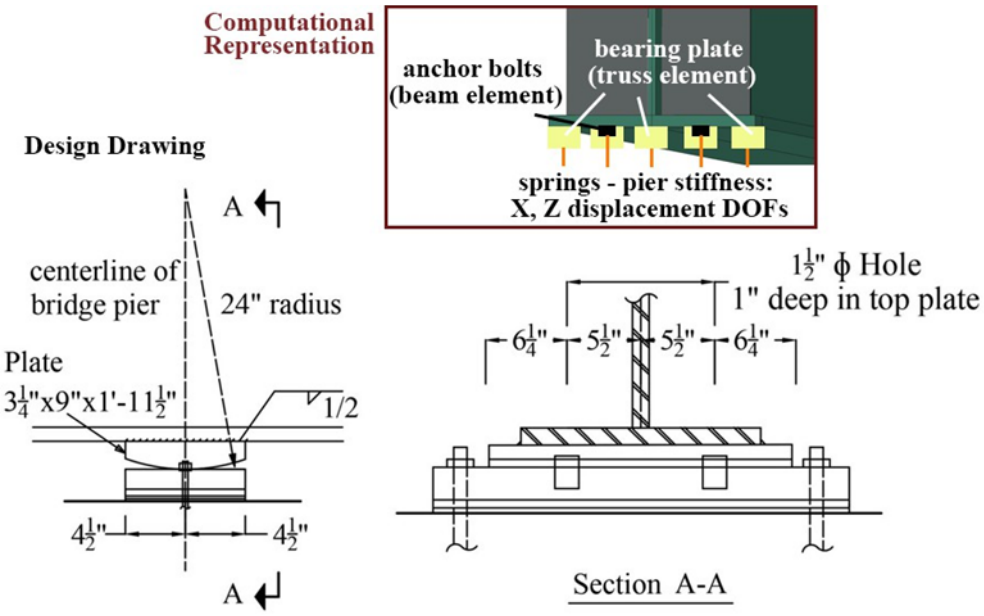

Figure 34. Illustration. Girder middle support condition of Mattis-74.

Bridge middle (pier) support was modeled as the girder bottom flange sitting on bearing plates and anchor bolts, then supported by the bridge pier. The bearing plate was represented as circular compression-only steel truss elements along the girder bottom flange at the bearing stiffener, and a pair of anchor bolts were defined as circular steel beam elements at the middle of the flange on both west and east sides. As an example, for Mattis-74 (as presented in Figure 34), each truss element was 11.4 cm (4.5 in.) in diameter and 8.3 cm (3.25 in.) long (representing bearing plate thickness) according to the design, and the bolts were 2.5 cm (1 in.) long and 3.8 cm (1.5 in.) in diameter. The dimensions were typical for pier-girder connections in a continuous-span bridge. For example, Mattis-57 has an identical design with slightly different bearing plate size. The elements were pinned (restrained in all displacement dofs) to the girder bottom flange at one side and were restrained in all rotational and *Y*-direction displacement dofs at the other side. The connection to the ground in the *X* and *Z* displacement directions was established through springs in *X* and *Z* displacement dofs that represent the bridge pier's flexibility. Spring stiffnesses were determined by treating the pier system as an individual structure. Load was applied in parallel and perpendicular to skew directions on the top of the pier and fixed boundary conditions in all dofs at the bottom of the pier.

LOADING AND DATA EXTRACTION

Live load truck testing and deck placement were simulated in ABAQUS using a DLOAD user subroutine, with static load steps representing slow-speed truck testing and concrete pouring. Truck wheels were defined as 50 cm by 25 cm (20 in. by 10 in.) areas of pressure (AASHTO 2017), applied to the concrete deck. Wet concrete was placed along the skew, applied on the wooden formwork and girder top flanges. Local coordinates were adjusted to properly extract normal stress from elements of interest. A five-point through-thickness Simpson's Rule integration was used for all S4R elements. Section points SP1 and SP5 were extracted for normal stresses representing the bottom and top surfaces of the shell elements, respectively. Temperature varied slightly, both during the continuous

deck placement over a few hours and during a live load test with a weighed vehicle, so thermal effects were not considered in the abovementioned short-term analysis.

Construction live load was not considered in the analysis of the deck placement process. Parametric studies conducted for model validation showed that weight from the screed machine along bridge edges (the major portion of live load) only leads to a small improvement in field-model agreement for exterior girders. Distribution of other live loads from equipment and personnel varies depending on pouring sequence, and it only contributes to analysis results regionally. Prior research found that consideration of concrete hardening during deck placement does not affect model accuracy, but analysis results are more significantly affected by boundary conditions (Choo et al. 2005), which were carefully iterated as described in the prior section. Strain variation in the bridge superstructure during concrete placement was analyzed, but bridge response that occurred before the deck pour was not considered. Steel dead load fit detailing was used for construction of the Mattis Avenue bridges and is typical practice for bridges in Illinois (M. Shaffer, pers. comm., 2022). The bridges were modeled with linear elastic material properties under concrete dead load, and geometric nonlinearity—proven to provide insignificant improvement in accuracy of field-model agreement—was not included.

CHAPTER 5: BRIDGE PRELIMINARY ANALYSIS

Response prediction of selected bridges is essential for determining critical girder cross-sections and cross-frames for instrumentation so that superstructure load transfer can be captured accurately in the field. Preliminary finite element analysis of the instrumented bridges (presented in Chapter 3) was conducted for planning the field instrumentation. A modeling framework was validated with prior field monitoring by other researchers, which was similar to but slightly simpler than that presented in Chapter 4.

NUMERICAL MODELING OF A PREVIOUSLY MONITORED BRIDGE

Bridge US-13, which was studied by McConnell et al. (2014), has similar geometry to the bridges in the current research. US-13 was modeled in the current work using ABAQUS (2017), and truck tests were simulated for cases conducted in the field by McConnell et al. (2014). In addition to confirming the validity of the modeling framework, these simulations provided initial insight into load distribution in skewed steel I-girder bridge superstructures, which informed decisions about instrumentation in the current research.

Introduction of the Monitored Bridge from Prior Research

US-13 is a two-span continuous stub abutment bridge in Delaware. It has 65° skew, X-shaped cross-frames, and five 1.7 m (66 in.) deep steel plate I-girders. Figure 35 presents an instrumentation plan view for US-13. Similarity in geometry between US-13 and Mattis-74 makes it a reasonable choice for preliminary numerical study, which can validate modeling methodologies and provide understanding of typical behavior for continuous-span skewed steel I-girder bridges at an early stage of the research. Three truck passes were conducted as part of live load testing. The truck was moved farther away from the instrumented girder (G4) going from Pass 1 to Pass 3. The test truck had a front axle weight of 66 kN (14,780 lb) and middle and rear axle weights of 90 kN (20,250 lb). Details of the instrumentation layout and truck tests can be found in McConnell et al. (2014).

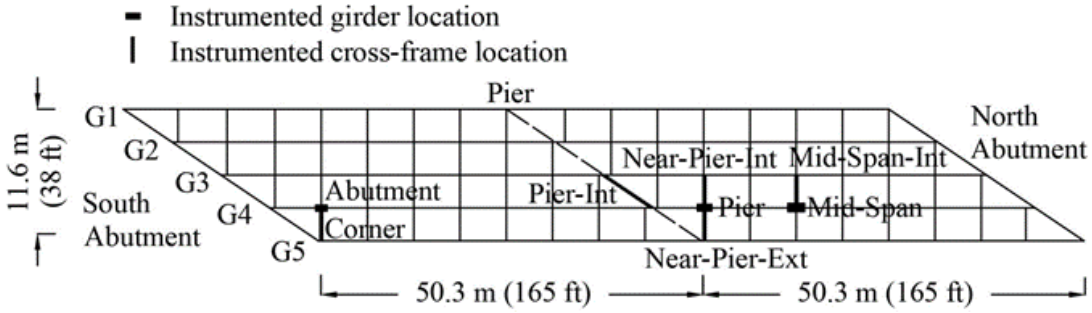

Figure 35. Plan view. Instrumentation of bridge US-13.

Source: Adapted from McConnell et al. (2016).

Three locations were instrumented along interior girder G4: near the pier, near one abutment, and near one mid-span location. Five cross-frames were instrumented: at an obtuse corner (Corner), at the pier in an interior bay (Pier-Int), near the pier in an exterior bay (Near-Pier-Ext), near the pier in

an interior bay (Near-Pier-Int), and at one mid-span location in an interior bay (Mid-Span-Int). Figure 36 presents instrumentation at typical girder cross-sections and cross-frames. The side of a cross-frame closer to the instrumented girder was monitored, and either gauge set A, C, E, G, I, and J or gauge set B, D, F, H, I, and J was instrumented at any particular cross-frame location. There could be strain gauges placed on one or both legs of angle members at the labeled locations.

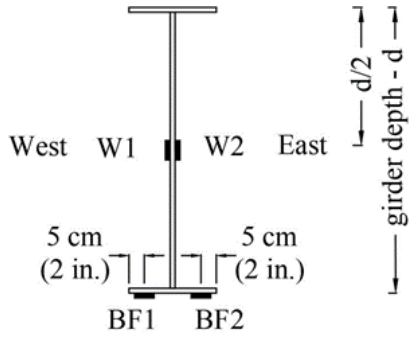

A. Girder cross-section

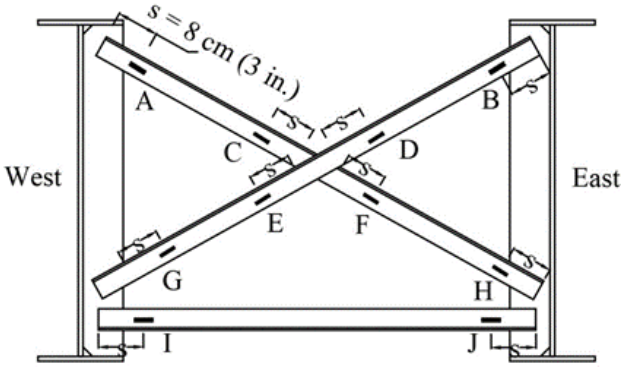

B. Cross-frame

Figure 36. Schematic. US-13 cross-sectional instrumentation layout.

Source: Adapted from McConnell et al. (2016)

Observation on Prior Field Results and Model Validation

McConnell et al. (2014) measured girder strain at the bottom flange and web and then evaluated strong-axis bending and lateral bending (assuming any axial force effect and local plate bending to be negligible). Strong-axis bending is the main source of in-plane behavior for an I-girder, and lateral bending comprises a combination of weak-axis bending and cross-flange bending due to restrained warping. For every instrumented girder cross-section during each test, the maximum tensile and compressive strains of the two gauges on the bottom flange were extracted—either at location BF1 or BF2—and a reading was taken from the other gauge at the same time to form a "concurrent dataset." An average of the two normal stresses (calculated assuming linear elastic behavior from the strain readings) in a concurrent dataset estimates the extreme fiber strong-axis bending stress of the bottom flange, and half the difference between the two normal stresses represents the lateral bending stress at the gauge location (5 cm [2 in.] from the outside tip of the bottom flange). A similar concept was used to record pairs of readings at girder web gauges, from which strong-axis bending

stress and lateral bending stress at the girder web were evaluated. Extreme cases of strong-axis bending and lateral bending are well captured at the observation of maximum strains with this method. Next, numerical simulation results using models developed for the current research by the authors are presented and compared to field data from McConnell et al. (2014). The modeling framework using ABAQUS developed through validation during the analysis, as a slightly simpler preliminary set of numerical simulation, was similar to that described in Chapter 4.

Figure 37 (bottom flange) and Figure 38 (web) compare field measurement and numerical simulation results for maximum normal stress due to strong-axis bending and lateral bending under truck Pass 1. These comparisons are representative of field-simulation agreement for all three truck tests. The magnitude of stress from both maximum tensile (positive) and compressive (negative) concurrent datasets for all instrumented girder cross-sections are presented in the figures.

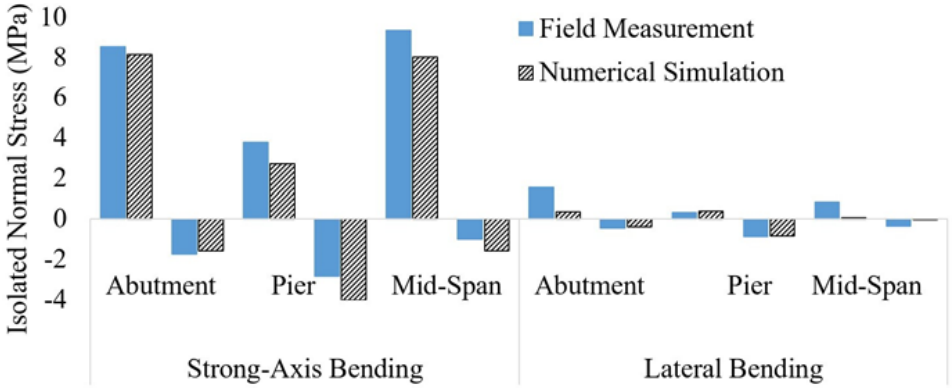

Figure 37. Graph. Comparison of decomposed maximum normal stress at girder bottom flange during Pass 1.

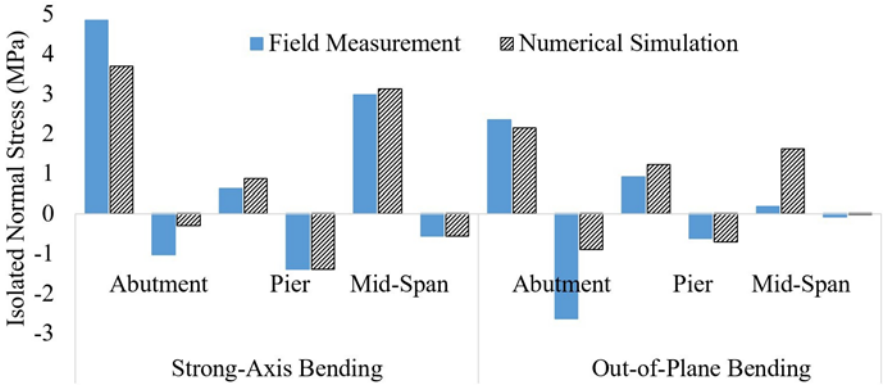

Figure 38. Graph. Comparison of decomposed maximum normal stress at girder web during Pass 1.

Overall, the model reasonably captured responses at the girder cross-sections, especially regarding maximum normal stress due to strong-axis bending, and the models used in the current study produced results that agree with the field data at least as well as those developed previously by McConnell et al. (2014). The relatively larger difference for lateral stress between numerical simulation and field measurement could result from unknown initial imperfections that are not

included in the model. Also, the field-monitored girder cross-sections of US-13 were relatively close to cross-frames, so effects from load transfer at cross-frames might result in local effects that are not considered in the assumptions made when conducting stress calculations using field strain measurements. The current research is focusing on girder instrumentation farther away from cross-frames to better capture global behavior and minimize localized effects. As described in Chapter 3, a more detailed strain measurement approach is also considered in the current research to more rigorously decompose sources of girder stress.

Cross-frame angle members were monitored in both concentric (connected) and eccentric (not connected) legs at some cross-frames during field monitoring of US-13. Concentric legs almost always had larger maximum stress than eccentric legs, so concentric legs are the focus of instrumentation in the current research. Element normal stress on concentric legs at the instrumented locations from field measurement and numerical simulation are compared, as presented in Figure 39 from truck Pass 1, which is representative of all three truck testing passes. Comparisons are made for both maximum tensile (positive) and compressive (negative) normal stress.

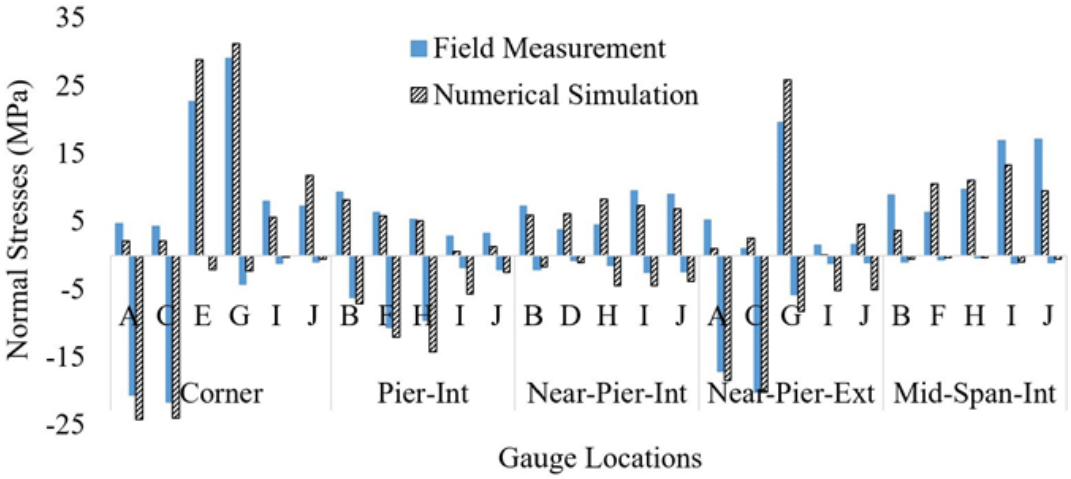

Figure 39. Graph. Comparison of decomposed maximum normal stress at girder web during Pass 1.

Modeling results reasonably represent the field data at most of the monitored cross-frame locations. Diagonal members are where relatively large normal stresses were captured among the instrumented cross-frames, so concentric legs of diagonal members are chosen to be instrumented for the current research due to higher observed stress and better accuracy of modeling results, with the final installation locations chosen farther away from the end of the angle members (larger "s," as presented in Figure 36-B) to avoid measuring localized behavior close to the connection. The two monitoring locations on the bottom chord—I and J—had similar maximum normal stress, which indicates that bottom chords of cross-frames are mostly under axial force; thus, having one strain gauge on the bottom chord of interest was determined to be sufficient for the current research.

NUMERICAL MODELING FOR INSTRUMENTATION PLANNING

Numerical simulations for planning the field instrumentation focused on the stub abutment configuration (Mattis-74, Figure 5). Instrumentation for the integral abutment configuration (Mattis-

57, Figure 6) was developed based on geometric similarity between the two selected bridges, adjusting for more detailed monitoring near the abutment due to rotational restraint provided by the integral condition. Both Mattis-57 and Mattis-74 were constructed in three stages, where Stages I and II are each approximately half of the bridge and Stage III is a narrow closure pour; instrumentation focuses on Stage I.

To approximate a common traffic condition, a load representing a typical maximum Class 1 vehicle—6 m in length × 2 m in width (240 in. × 80 in.) and with a total weight of 27 kN (6,000 lb)—was individually applied to the Mattis-74 model along each of the four traffic lanes, as presented in Figure 40, with the centroid of the truck at the lane's centerline. Normal stress at mid-thickness of the girder bottom flange edge elements—near locations BF1 and BF2 presented in Figure 36-A—was recorded along the girder length of G1 through G6, which are in Stage I. Similarly, normal stress at mid-thickness of cross-frame diagonal members (near Locations A and B presented in Figure 36-B) was extracted for all cross-frames at BAY 1 through BAY 5. Maximum tensile and compressive normal stress was recorded for every element during each pass, with the maximum normal stress of BF1 or BF2 taken as the maximum girder bottom flange normal stress for a section. Similarly, the maximum normal stress from location A or B is taken as the maximum cross-frame stress. Superposition of maximum stresses from vehicle Pass 1 through 4 then forms an envelope of stress for regular traffic loading considering a vehicle in each lane.

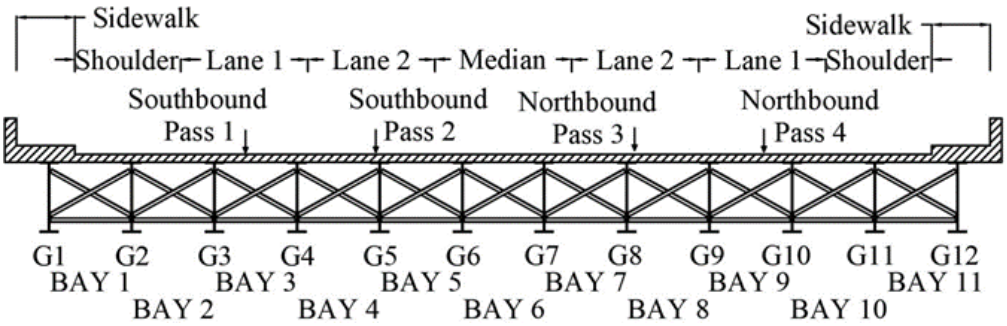

Figure 40. Section view. Load for preliminary analysis of Mattis-74.

Figure 41 presents the girder bottom flange stress envelopes for the traffic loads, where maximum normal stress is presented along the girder length. G5 and G4 were observed with the largest bottom flange tensile stress within the bridge span and, therefore, were chosen to be heavily instrumented. G3 and G6 were observed to have smaller stress magnitudes, so G3 was lightly monitored. G1 and G2 have relatively small responses and so only G1 was lightly monitored, as an exterior girder, to capture a thorough picture of global stress distribution. Maximum positive bending behavior was captured near CF3 for each girder in the south span and near CF12 in the north span. Overall, the north span had larger responses than the south span, which is reasonable due to its slightly longer span length, so instrumentation effort was focused on the north span of Mattis-74.

Figure 42 presents the normal stress envelopes of cross-frame diagonal members under the superimposed traffic load (combination of Pass 1 through Pass 4, as presented in Figure 40), which indicates there is no clear observation about where maximum tensile or compressive stress might be for cross-frames. With a focus on instrumentation of I-girders, the monitoring goal for cross-frames is

simply to capture load transfer within a bridge superstructure and track variation of cross-frame response over time. Monitoring cross-frames adjacent to girder cross-sections is therefore most beneficial, with cross-frames near corners of the skewed bridges also being of interest.

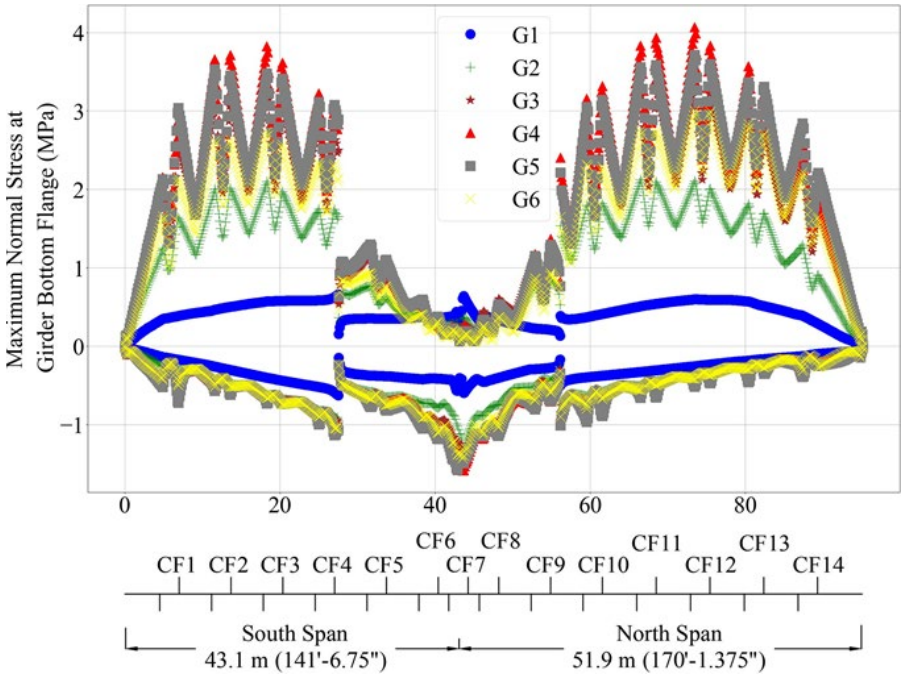

Figure 41. Graph. Girder bottom flange normal stress envelopes under superimposed traffic load (from preliminary numerical modeling).

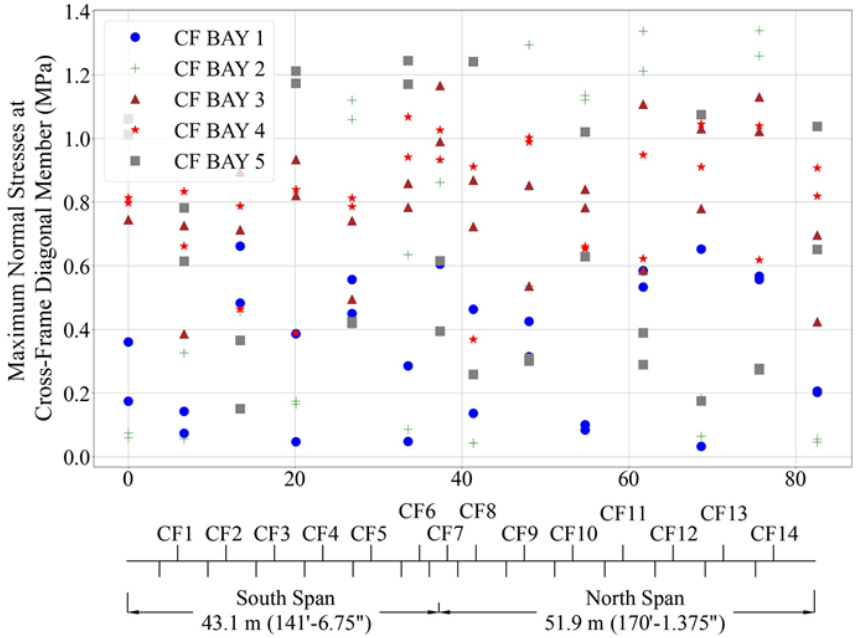

Figure 42. Graph. Cross-frame diagonal member normal stress envelopes under superimposed traffic load (from preliminary numerical modeling).

CHAPTER 6: SUMMARY

Highly skewed steel I-girder bridges are commonly used across the US, especially in congested areas, despite complexities in their analysis, design, and construction. Bridge superstructure behavior is complicated by the effects of skew due to additional load paths introduced via the skewed supports and through load transfer at cross-frames and the deck, both under construction and after bridges are in service. Field-monitoring efforts focusing on large-scale skewed steel I-girder bridge superstructures are sparse, and efficiency of standard design practice needs to be further evaluated through field monitoring and companion numerical studies. The current project was initiated in Illinois to investigate composite skewed I-girder bridge superstructure behavior during construction and after bridges are in service. Highly skewed stub abutment bridges and integral abutment bridges with steel I-girders were monitored in the field and analyzed with combined field measurements and numerical simulation under concrete dead load, traffic live load, and thermal load.

A survey was formulated and distributed across the US to understand practices used and challenges faced by state transportation agencies when designing and constructing skewed steel I-girder bridges. Findings from the survey responses illuminate issues, concerns, and current practices related to design, construction, and service life of those bridges. The agency survey guided the objectives of the research and informed the selection of two bridges in Champaign, Illinois, for field monitoring, in order to provide enhanced understanding of the effects of skew on bridge superstructure behavior. Two steel I-girder bridges skewed 41° and 45°, one with stub abutments and the other with integral abutments, respectively, were monitored in the field during construction and after bridges are in service. Critical girder cross-sections and cross-frames were instrumented with strain gauges using a data acquisition system with a high sampling frequency (up to 20 Hz). In addition, key girder end rotations and all bridge corner movements were monitored. Temperature variation was recorded with all sensors. Three-dimensional finite element analysis methods have been improved through iterations of model validation after field monitoring was started. Prior to the start of data collection, numerical simulation techniques were initially validated with prior research, and preliminary analysis was conducted on the selected bridge to guide field instrumentation planning.

Field monitoring entered a phase of steady long-term data collection since January 2021. The behavior of the two Mattis Avenue bridges was investigated through continuous analysis based on field data, accompanying field inspections, and periodic conventional surveys, which are discussed in subsequent report volumes of this project. Numerical simulations were conducted simultaneously to understand the response of the monitored bridges and expand knowledge on skewed steel I-girder bridges through parametric studies, which is also discussed extensively in other report volumes.

REFERENCES

ABAQUS/CAE. (2017). Dassault systems. V´elizy-Villacoublay, France: ABAQUS/CAE.

Aktan, H. M., & Attanayake, U. (2020). *Bridge structural analyses for staged construction and constructability reviews* (Report No. SPR-1691). Wayne State University/Michigan Department of Transportation.

Almoosi, Y., McConnell, J., & Oukaili, N. (2021). Evaluation of the variation in dynamic load factor throughout a highly skewed steel I-girder bridge. *Engineering, Technology and Applied Science Research*, *11*(3), 7079–7087. https://doi.org/10.48084/etasr.4106

American Association of State Highway and Transportation Officials (AASHTO). (2017). *Load and resistance factor design bridge design specifications, 8th edition*. Practice Periodical on Structural Design and Construction.

Australia Standard. (2004). *Bridge design – part 4: Bearings and deck joints*.

Azizinamini, A., Swendroski, J. P., & Yakel, A. (2003). *Development of a design guideline for phase construction of steel girder bridges* (Report No. SPR-PL-1). University of Nebraska Lincoln, Nebraska Department of Roads.

Barbaros, A., & Sevket, A. (2017). Determination of bearing type effect on elastomeric bearing selection with SREI-CAD. *Advances in Computational Design*, *2*(1), 43–56. https://doi.org/10.12989/ACD.2017.2.1.043

Barr, P. J., Eberhard, M. O., & Stanton, J. F. (2001). Live-load distribution factors in prestressed concrete girder bridges. *Journal of Bridge Engineering*, *6*(5), 298–306. https://doi.org/10.1061/(ASCE)1084-0702(2001)6:5(298)

Campbell Scientific, Inc. (2022). Logan, UT. www.campbellsci.com.

Choi, W., Mohseni, I., Park, J., & Kang, J. (2019). Development of live load distribution factor equation for concrete multicell box-girder bridges under vehicle loading. *International Journal of Concrete Structures and Materials*, *13*(22). https://doi.org/10.1186/s40069-019-0336-1

Choo, T. W., Linzell, D. G., Lee, J. I., & Swanson, J. A. (2005). Response of a continuous, skewed, steel bridge during deck placement. *Journal of Constructional Steel Research*, *61*(5), 567–586. https://doi.org/10.1016/j.jcsr.2004.10.009

Clifton, S. P., & Bayrak, O. (2008). *Bridge deck overhang construction* (Report No. IAC 88-5DD1A003-2). The University of Texas at Austin, Texas Department of Transportation.

Clough, G. W., & J. M. Duncan (1990). Earth pressures. In Fang, H.-Y. (Ed.), *Foundation Engineering Handbook* (pp. 223-235). Springer. https://doi.org/10.1007/978-1-4615-3928-5_6

Deng, L., Yu, Y., Zou, Q., & Cai, C. S. (2015). State-of-the-art review of dynamic impact factors of highway bridges. *Journal of Bridge Engineering*, *20*(5), 04014080. https://doi.org/10.1061/(ASCE)BE.1943-5592.0000672

Deng, Y., & Phares, B. M. (2016). *Investigation of the effect of speed on the dynamic impact factor for bridges with different entrance conditions* (InTrans Project 14-521). Bridge Engineering Center,

Iowa State University.

Dicleli, M., & Yalcin, O. F. (2018). Incorporation of skew effects in live-load distribution factors developed for typical integral bridges. *Journal of Bridge Engineering*, *23*(2), 04017135. https://doi.org/10.1061/(ASCE)BE.1943-5592.0001188

Ensoft. (2017). "LPILE Plus 5.0 Geotechinical Analysis Program (student version)." Austin, TX.

Fahnestock, L. A., Chee, M., Liu, G., Kode, U., & LaFave, J. M. (2022). Synthesis of bridge approach slab behavior, design, and construction practice. *Practice Periodical on Structural Design and Construction*, *27*(3), 04022032. https://doi.org/10.1061/(ASCE)SC.1943-5576.0000704

Florida Department of Transportation (FDOT). (2021). *Structures design guidelines*. FDOT.

Freeseman, K., Phares, B., Shafei, B., & Kulkarni, A. (2014). Investigation of exterior girder rotation and the effect of skew during deck placement.

Gent, A. N. (2012). *Engineering with rubber: How to design rubber components, 3rd edition*. Hanser Publications.

Geokon, Inc., (2022). Lebanon, NH. www.geokon.com.

Greimann, L., Phares, B. M., Deng, Y., Shryack, Y., & Hoffman, J. (2014). *Field monitoring of curved girder bridges with integral abutments* (InTrans Project 08-323). Bridge Engineering Center, Iowa State University.

Huang, D. (2001). Dynamic analysis of steel curved box girder bridges. *Journal of Bridge Engineering*, *6*(6), 506–513. https://doi.org/10.1061/(ASCE)1084-0702(2001)6:6(506)

Huang, D., Wang, T.-L., & Shahawy, M. (1995). Dynamic behavior of horizontally curved i-girder bridges. *Computers and Structures*, *57*(4), 703–714. https://doi.org/10.1016/0045-7949(95)00061-K

Illinois Department of Transportation (IDOT). (2012). *Bridge manual*. IDOT.

Illinois Department of Transportation (IDOT). (2023). *Bridge manual*. IDOT.

Ishii, K., Kikuchi, M., Nishimura, T., & Black, C. J. (2016). Coupling behavior of shear deformation and end rotation of elastomeric seismic isolation bearings. *Earthquake Engineering and Structural Dynamics*, 46(4), 677–694. https://doi.org/10.1002/eqe.2809

Khaloo, A. R., & Mirzabozorg, H. (2003). Load distribution factors in simply supported skew bridges. *Journal of Bridge Engineering*, *8*(4), 241–244. https://doi.org/10.1061/(ASCE)1084-0702(2003)8:4(241)

Krupicka, G., & Poellot, B. (1993). Nuisance stiffness. *HDR Bridgeline*, *4*(1), 3.

LaFave, J. M., Brambila, G., Kode, U., Liu, G., & Fahnestock, L. A. (2021). Field behavior of integral abutment bridges under thermal loading. *Journal of Bridge Engineering*, *26*(4), 04021013. https://doi.org/10.1061/(ASCE)BE.1943-5592.0001677

LaFave, J. M., Riddle, J. K., Jarrett, M. W., Wright, B. A., Svatora, J. S., An, H., & Fahnestock, L. A. (2016). Numerical simulations of steel integral abutment bridges under thermal loading. *Journal of Bridge Engineering*, *21*(10), 04016061. https://doi.org/10.1061/(ASCE)BE.1943-5592.0000919

McConnell, J., Radovic, M., & Ambrose, K. (2014). *Cross-frame forces in skewed steel i-girder bridges: Field measurements and finite element analysis* (Report No. DCT 241). University of Delaware, Delaware Center for Transportation.

McConnell, J. R., Radovic, M., & Ambrose, K. (2016). Field evaluation of cross-frame and girder live-load response in skewed steel i-girder bridges. *Journal of Bridge Engineering*, *21*(3), 04015062. https://doi.org/10.1061/(ASCE)BE.1943-5592.0000846

McConnell, J., Radovic, M., & Keller, P. (2020). Holistic finite element analysis to evaluate influence of cross-frames in skewed steel i-girder bridges. *Engineering Structures*, *213*, 110556. https://doi.org/10.1016/j.engstruct.2020.110556

Mitoulis, S. A. (2015). Uplift of elastomeric bearings in isolated bridges subjected to longitudinal seismic excitations. *Structure and Infrastructure Engineering*, *11*(12), 1600–1615. https://doi.org/10.1080/15732479.2014.983527

Mohseni, I., Cho, Y. K., & Kang, J. (2018). Live load distribution factors for skew stringer bridges with high-performance-steel girders under truck loads. *Applied Sciences*, *8*(10). https://www.mdpi.com/2076-3417/8/10/1717

Morera, F., & Sumner, E. A. (2020). *Lateral flange bending in heavily skewed steel bridges* (Report No. Report FHWA/NC/2007-09). North Carolina State University, North Carolina Department of Transportation.

Nebraska Department of Roads (NeDOR). (2016). *Bridge office policies and procedures*. NeDOR.

Nouri, G., & Ahmadi, Z. (2012). Influence of skew angle on continuous composite girder bridge. *Journal of Bridge Engineering*, *17*(4), 617–623. https://doi.org/10.1061/(ASCE)BE.1943-5592.0000273

Olson, S. M., Holloway, K. P., Buenker, J. M., Long, J. H., & LaFave, J. M. (2013). *Thermal behavior of IDOT integral abutment bridges and proposed design modifications* (Report No. FHWA-ICT-12-022). Illinois Center for Transportation/Illinois Department of Transportation.

Pennsylvania Department of Transportation (PennDOT). (2016). *Standard cross-frame and solid plate diaphragms for steel beam/girder bridges designed with refined methods of analysis*. PennDOT.

Pennsylvania Department of Transportation (PennDOT). (2019). *Design manual, part 4 (dm-4) structures: Procedures–design–plans presentation pdt*. PennDOT.

Razzaq, M. K., Sennah, K., & Ghrib, F. (2021). Live load distribution factors for simply-supported composite steel I-girder bridges. *Journal of Constructional Steel Research*, *181*, 106612. https://doi.org/10.1016/j.jcsr.2021.106612

Reese, L. C., & Welch, R. C. (1975). Lateral loading of deep foundations in stiff clay. *Journal of the Geotechnical Engineering Division*, *101*(7), 633–649. https://doi.org/10.1061/AJGEB6.0000177

Reis, L. C., Krahl, P. A., & Lima, M. C. V. (2020). Numerical analysis of the effective stiffness of elastomeric bearing pads under precast beams for the limit load of lateral instability. *Revista IBRACON de Estruturas e Materiais*, *13*(1), 95–119. https://doi.org/10.1590/s1983-41952020000100008

Roeder, C. W., Stanton, J. F., & Taylor, A. W. (1987). *Performance of elastomeric bearings* (NCHRP No. 298). National Cooperative Highway Research Program.

Sağlık, H., Doran, B., & Balkaya, C. (2018). Investigation of natural frequency for continuous steel bridges with variable cross-sections by using finite element method. *International Journal of Engineering Technologies*, *4*(2), 90–102.

Salah, A. A. N. (2020). Numerically modeling steel continuous bridges for early age concrete deck cracking. Master's thesis, University of Arkansas.

Sanchez, T. A. (2011). Influence of bracing systems on the behavior of curved and skewed steel I-girder bridges during construction. Doctoral thesis, Georgia Institute of Technology.

Shamsabadi, A., Rollins, K. M., & Kapuskar, M. (2007). Nonlinear soil-abutment-bridge structure interaction for seismic performance-based design. *Journal of Geotechnical and Geoenvironmental Engineering*, *133*(6), 707–720. https://doi.org/10.1061/(ASCE)1090-0241(2007)133:6(707)

Steelman, J. S., Fahnestock, L. A., Filipov, E. T., LaFave, J. M., Hajjar, J. F., & Foutch, D. A. (2013). Shear and friction response of nonseismic laminated elastomeric bridge bearings subject to seismic demands. *Journal of Bridge Engineering*, 18(7), 612‑623. https://doi.org/10.1061/(ASCE)BE.1943-5592.0000406

Steelman, J. S., Fahnestock, L. A., Hajjar, J. F., & LaFave, J. M. (2018). Cyclic experimental behavior of nonseismic elastomeric bearings with stiffened angle side retainer fuses for quasi-isolated seismic bridge response. *Journal of Bridge Engineering*, *23*(1), 04017120. https://doi.org/10.1061/(ASCE)BE.1943-5592.0001170

Terzioglu, T., Hueste, M. B. D., & Mander, J. B. (2017). Live load distribution factors for spread slab beam bridges. *Journal of Bridge Engineering*, *22*(10), 04017067. https://doi.org/10.1061/(ASCE)BE.1943-5592.0001100

Theoret, P., Massicotte, B., & Conciatori, D. (2012). Analysis and design of straight and skewed slab bridges. *Journal of Bridge Engineering*, 17(2), 289–301. https://doi.org/10.1061/(ASCE)BE.1943-5592.0000249

Texas Department of Transportation (TxDOT). (2018). *Bridge design manual — LRFD*. TxDOT.

Texas Department of Transportation (TxDOT). (2019). *Miscellaneous details steel girders and beams*. TxDOT.

Utah Department of Transportation (UDOT). (2017). *Structures design and detailing manual*. UDOT.

URS Corporation. (2016). Study of skewed rolled-beam bridges for evaluation of diaphragm forces and exterior beam live load distribution factors and a recommendation of line analysis skewed limit.

White, D., Coletti, D., Chavel, B., Sanchez, A., Ozgur, C., Chong, J., Leon, R., Medlock, R., Cisneros, R., Calambos, T., Yadlosky, J., Gatti, W., & Kowatch, G. (2012). *Guideline for analysis methods and construction engineering of curved and skewed steel girder bridges*.

White, D., & Jamath, A. (2020). *Straight steel i-girder bridges with skew index approaching 0.3*. Heath and Lineback Engineers, Inc., Florida Department of Transportation.

Yang, S., Helwig, T., Klingner, R., Engelhardt, M., & Fas, J. (2010). *Impact of overhang construction on girder design* (Report No. FHWA/TX-10/0-5706-1). Center for Transportation Research, Texas Department of Transportation.

Zhou, S., Fahnestock, L. A., & LaFave, J. M. (2023). Development of skewed steel I-girder bridge field monitoring strategy through agency survey and numerical simulation. *Practice Periodical on Structural Design and Construction*, *28*(1), 04022056. https://doi.org/10.1061/(ASCE)SC.1943-5576.0000740

Zhou, S., Fahnestock, L. A., LaFave, J. M., & Dorado, R. (2022). Construction and live load behavior of a skewed steel I-girder bridge. *Transportation Research Record*, *2678*(1), 03611981221105276. https://doi.org/10.1177/03611981221105276


Illinois Department
of Transportation


ILLINOIS